Discrete Element Modeling of Railway Ballast for Studying Railroad Tamping Operation

Ashish Jain

Thesis submitted to the faculty of the

Virginia Polytechnic Institute and State University

in partial fulfillment of the requirements for the degree of

Master of Science

in

Mechanical Engineering

Mehdi Ahmadian, Chair

Steve C Southward

Reza Mirzaeifar

December 2017

Blacksburg, Virginia, USA

Keywords: Discrete Element Modeling, DEM, railway ballast, track settlement, tamping, track stability, contact model, particle shape, ballast compaction, coordination number.

Discrete Element Modeling of Railway Ballast for Studying Railroad Tamping Operation

Ashish Jain

Abstract

The development of Discrete Element Model (DEM) of railway ballast for the purpose of studying the behavior of ballast particles during tamping is addressed in a simulation study, with the goal of optimizing the railroad tamping operation. A comprehensive literature review of applicability of DEM techniques in modeling the behavior of railway ballast is presented and its feasibility in studying the fundamental mechanisms that influence the outcome of railroad tamping process is analyzed. A Discrete Element Model of railway ballast is also developed and implemented using a commercially available DEM package: PFC^{3D}. Selection and calibration of ballast parameters, such as inter-particle contact force laws, ballast material properties, and selection of particle shape are represented in detail in the model. Finally, a complete tamping simulation model is constructed with high degree of adjustability to allow control of all process parameters for achieving realistic output.

The analysis shows that DEM is a highly valuable tool for studying railroad tamping operation. It has the capability to provide crucial and unprecedented insights into the process, facilitating not only the optimization of current tamping practices, but also the development of novel methods for achieving sustainable improvements in track stability after tamping in the future. Different ways of modeling particle shapes have been evaluated and it has been shown that while using spheres to represent irregular ballast particles in DEM provides immense gains in computational efficiency, spheres cannot intently capture all properties of irregularly shaped particles, and therefore should not be used to model railway ballast particles. Inter-particle and wall-particle contact forces are calculated using Hertzian contact mechanics for determining ballast dynamics during tamping. The results indicate that the model is able to accurately predict properties of granular assemblies of the railway ballast in different test cases. The developed model for simulating tamping operation on a half-track layout is expected to be extended in future studies for evaluating rail track settlement and stability, optimization of tamping process, and performance of different ballast gradations.

Discrete Element Modeling of Railway Ballast for Studying Railroad Tamping Operation

Ashish Jain

General Audience Abstract

Development of a virtual simulation model for the stone bed which forms the foundation of traditional rail track structures is discussed in this study for the purpose of improving a conventional railway maintenance practice called tamping. The stone bed, called ballast, is flexible and is susceptible to undesirable deformation due to the forces from train traffic on the rail tracks over their service time. Therefore, periodic restoration of track structure is performed by tamping to maintain the operational quality of the rail tracks and reduce the risk of train accidents. This simulation model is intended to accelerate the scientific development of the current tamping practices by providing unprecedented insight into the behavior of small stones which form the bulk of the ballast and obviating the requirement for costly physical experimentation. The nuances of the mechanical behavior of ballast have been examined by a comprehensive literature review and the selection of a modeling technique called Discrete Element Modeling (DEM) has been justified for modeling of ballast owing to its suitability in capturing intricate dynamics of ballast stones.

The virtual simulation model which is developed as results of this work has been found to be extremely efficient in realistically predicting the outcome of tamping process for any set of conditions of interest. This implies that quality of the rail tracks after tamping can be studied for a variety of different test cases and most optimized set of tamping parameters which results in maximum track quality can be analyzed. However, it was observed that the accuracy of the results obtained from the simulation model is dependent on the level of detail which is used to input properties of the ballast into the model. Low level of detail results in less accurate results whereas a high level of detail takes an unreasonably long time to solve. Therefore, a compromise has to be made between accuracy and solution time while programming the simulation model, and additional work is required in the future to improve the solution speed of the model.

To my teachers, family, and friends

Acknowledgement

This research effort would not have been accomplished without the sapient guidance and relentless contribution from a number of people. I am eternally grateful to Dr. Mehdi Ahmadian for his unequivocal support, mentorship, and encouragement throughout my studies at Virginia Tech. I would also like to sincerely thank the other members of my committee, Dr. Steve Southward and Dr. Reza Mirzaeifar for their unabating counsel and supervision on this project.

My time at Virginia Tech would not have been successful and fruitful without my colleagues at the Center for Vehicle Systems and Safety. I express my gratitude to Dr. Andrew Peterson, Dr. Masood Taheri, Sara Vallejo, Dr. Yang Chen, Dr. Yunbo Hou, Andrew Kim, Dejah Singh, Zebo Zhu, Yashvardhan Gupta, Karan Kothari, Jay Dixit, Liang Sun, Guankuan Jiao, and Gibran Ali for their companionship and endorsement.

Learning Experience Design (LED) at Virginia Tech and Derrick Blanksma from ITASCA Consulting Group also deserve a special mention for their technical support to this project.

Finally, I am forever indebted to my parents and my sister for their invaluable confidence in me and selfless support in all areas of my life.

Contents

List of Figures

List of Tables

1. Introduction

1.1 Motivation

Railroads around the world annually spend several billion dollars, roughly 20% of their budget, on maintenance of their existing infrastructure and assets, and approximately 58% of that is spent on maintenance of track and substructure [1]. Tamping is a track maintenance activity that is used for elimination of defects in the track geometry and correcting spatial alignment of rail tracks. It is one of the major activities that influence overall track maintenance costs for the railroads, and in combination with other regular maintenance activities such as rail grinding, can potentially lead to annual savings of about $9,500 per mile of railway track in other areas of maintenance [1]. However, traditional tamping practices are slow and lead to reduction in track availability by occupying revenue service time. Furthermore, optimal procedure of tamping is often deemed disputable by the experts [2]. Even though the effects of various parameters of the tamping process such as the vibration frequency, amplitude, depth of insertion into the ballast, etc. on resulting compaction of ballast below the sleeper have been investigated in the past, there is a persistent lack of consensus on what constitutes an optimum tamping cycle. American railroad companies primarily rely on the tamping equipment manufacturers for aggrandizement of tamping technology [3], but different manufacturers claim conflicting practices as favorable. For example, three different tamping equipment manufacturers have claimed different tamping frequencies as optimum- 35Hz, 42Hz and 50Hz. Machines made by these manufacturers also differ in design of their tamping tools (tines) and the nature of vibration used while insertion of tines into the ballast. Consequently, advancement of tamping techniques is an area of key research interest for the railroad companies.

Innovation in railroad tamping has customarily been based on empirical and semi-empirical methods of scientific development, mainly due to lack of reliable theoretical models for prediction of dynamics of complex granular systems like railway ballast. Several researchers have

constructed experiments with full-sized or scaled apparatus ([4], [5], [6], etc.), and have collected track alignment data over long periods of time to develop mathematical models for grossly accurate prediction of track settlement. Such research methodologies often have long incubation periods, require high capital investment, and yield results over the course of years, making them the prerogative of a select few. Moreover, fundamental properties that influence the output of tamping, such as ballast compaction, cannot be practically measured in realistic conditions. However, latest advancements in modeling of complex granular systems based on high computational power of modern processing units have fast-tracked the development of railroad tamping as well. Discrete Element Modeling (DEM) techniques, developed in early 1980s by Cundall [7], have proven to be a powerful way of gaining insight into dynamics of disordered granular systems and within the last decade, many researchers across the world have employed DEM to simulate railway ballast in diverse settings with encouragingly high levels of accuracy. Work presented in this thesis spearheads the development of the Virginia Tech's RTL Virtual Ballast model, which will be used for advanced studies focused around the dynamics of railway ballast in the future, including tamping.

1.2 Objectives of the Research

The goal of this project was to develop a simulation model to understand granular dynamics of the railway ballast for facilitating the study of railroad tamping operation and eventually, other phenomena related to track alignment, track stability, ballast gradations, and ballast degradation.

This goal was accomplished by realizing all the following objectives-

1. Provide effective means for modeling tamping dynamics, as it is practiced in the railway industry for increasing track stability;
2. Evaluate modeling means that can accurately and adequately represent tamping dynamics;
3. Determine the limitations of the selected models, in terms of error, run time, complexity to set up, and any difficulties in conducting parametric studies;
4. Run test cases that provide a pathway for future studies that can help with improving tamping practices.

1.3 Adopted Approach

The project objectives described in the previous section were fulfilled by adopting an approach involving the execution of the following tasks-

1. Adjudge the applicability of DEM techniques in studying the behavioral dynamics of railway ballast in a scientifically sound manner.
2. Conduct a literature survey for investigating the latest and the most feasible DEM practices, particularly suited for simulation of railway ballast.
3. Select a suitable DEM software package and associated computer hardware per the software requirements.
4. Prepare a model for the railway ballast using the software and calibrate model parameters for accuracy of physics.
5. Extend the railway ballast model to include a full tamping simulation model.

Discrete Element Modeling was not only found to be useful for studying the ballast dynamics, but evidently also provided invaluable insight into the granular physics that was beyond the scope of experimental investigation. It allows determination of certain physical properties of granular systems that cannot be measured in practice. Effects of unquantifiable variables like particle shape and angularity on resulting dynamics could also be studied with the help of DEM.

Literature survey revealed that there are different type of modeling methodologies and only a few of them are suited for modeling of railway ballast. These methods differ in functionality depending on the nature of granular assembly being studied- like magnitude of particle velocities, frequency of inter-particle collisions, density of packaging of particles in the assembly, etc. For conciseness, other modeling methodologies that were not suitable for use will not discussed in this document.

Analysis of costs, functionality, features, usability, versatility, and customer support followed the literature survey and PFC^{3D} from ITASCA Consulting Group, Inc. was chosen as the software package of choice. A processing unit was also set-up based on the specified system requirements for the software. A DEM model for the railway ballast was then prepared, and various model parameters like material properties, inter-body and inter-particle contact physics, particle shape etc. were carefully calibrated for highest feasible accuracy in the results.

Lastly, a tamping simulation model was constructed by adding tamping tines and half-sleeper rail track to the ballast model. Various recorded output variables can yield time histories of different ballast properties of interest for set input behavior of tines and load of the rail track. Only the construction and execution of the tamping model in the simulation software has been covered as a part of this project.

1.4 Contributions

The results of this work directly contribute towards furtherance of knowledge and conventions in the field of railway ballast and track interaction in the following ways:

- Providing a better understanding of the application of Discrete Element Modeling techniques for modeling railway ballast.
- Establishing the critical elements of DEM methodology for modeling railway ballast, such as contact force laws, material properties, and particle gradations.
- Selection of appropriate particle shape in the simulation model to accurately capture granular dynamics of railway ballasts.
- Developing routines to replicate a given ballast sample into the simulation model using 3D scanning techniques.
- Construction of a complete simulation model to allow study of tamping process in a virtual environment.

Since these developments in the modeling domain reduce the dependence of technological growth on capital and time intensive experiments, they lead to shortening of design and development cycles. Thus, these contributions, in turn, have the potential to accelerate progress of numerous track design routines and maintenance activities. Consequently, not only the design practices for ballasted tracks are improved, but also significant cost savings result for railroad companies due to longer maintenance cycles.

1.5 Thesis Outline

Chapter 2 of this document presents and extensive literature review on track stability, tamping, and Discrete Element Modeling (DEM). It is shown that resultant track stability after tamping primarily is a function of state of ballast. And therefore, applicability and feasibility of DEM techniques in simulating ballast behavior and studying tamping has been discussed.

Chapter 3 discusses modeling of contact physics between pairs of bodies and selection of appropriate contact models for capturing realistic contact behavior of railway ballast. Mathematical formulation of conventionally used contact models has been presented and compared, and configuration of physical parameters involved in the mathematical formulation has been explained.

The effect of ballast particle shape and size distribution, called gradation, on track stability and results of DEM simulation has been presented in Chapter 4. A simulation study undertaken to compare performance of spherical and irregularly shaped ballast particles has been discussed, and conclusions drawn from the results of the study have been examined.

Chapter 5 described the construction of a tamping simulation model in a commercially available DEM package. The underlying assumptions of the model have been listed, and the information flow within the model has been discussed in detail. Lastly, the initial and boundary conditions, and the input and output variables of the model have been encapsulated.

Finally, Chapter 6 summarizes the results of this entire work and discusses the potential applications of the developed model of railway ballast beyond tamping, along with the steps required to continue the present work in the future.

2. Background

2.1 Railway Tracks and Tamping

2.1.1 Railway Tracks

The structure of railway tracks is composed of different components. A representation of cross-section of railway track structure is shown in Figure 2.1-

- Superstructure: It is the top most component of the structure and comprises of the rails, fasteners, and sleepers. The two rails are the only parts that interact with the train wheels, and fasteners and sleepers are used to maintain rail position and alignment.
- Substructure: It comprises of ballast, sub-ballast and subsoil. Sleepers are simply supported by the ballast, therefore, this component transfers traffic loads from superstructure to the ground. Substructure is also responsible for maintaining alignment of the superstructure and provide drainage for water. Ballast and sub-ballast are granular aggregates of randomly crushed stones and are usually made of materials like basalt, granite, limestone, gravel, etc. Shape and size distribution of stones in the aggregate, called the gradation of the aggregate, is often regulated by the concerned authorities.

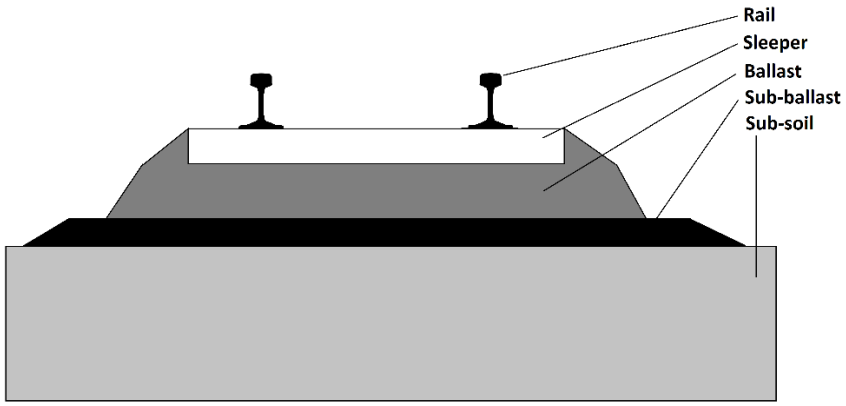

Figure 2.1 Components of the structure of ballasted railway tracks.

2.1.2 Track Settlement and Stability

Due to repeated loading from circulating traffic, non-uniform consolidation of ballast occurs below the sleepers. As a result, numerous long wavelength defects are introduced in the track geometry [8] and the vertical alignment of the track is disturbed. This is called track settlement. Figure 2.2, sourced from [9], shows defects in the track geometry caused by settlement of the ballast.

Figure 2.2 Defects in railway track geometry caused by settlement of ballast, image sourced from [9].

Resistance of tracks to misalignment in vertical and lateral direction refers to track stability. Even though there are other factors that affect track stability such as thermal stresses, drainage, etc., it is primarily influenced by resistance provided to the displacement of sleepers by the ballast [1].

Track stability in the vertical direction is dependent on the compaction of ballast directly below the sleeper [1]. The higher the compaction, the lower the settlement of track below its initial level. Since there are no practical ways of determining ballast compaction below the sleepers experimentally, vertical track settlement is predominantly measured as amount of settlement over time or cumulative loading, or by manipulating compaction levels in the laboratory environment. Vertical track settlement is also a function of traffic speed, axle loads, and traffic density as these factors indirectly influence resistance from the ballast.

Thermal stresses and uneven forces in the lateral direction can lead to buckling of railway tracks in the lateral direction. Figure 2.3, sourced from [10], shows buckling of tracks due to high ambient

temperatures. Lateral track stability is the resistance of railway track to displacement in the lateral direction. It is influenced by the friction between ballast particles and sleepers, and normal resistance to lateral displacement of the sleepers by the ballast present at their end on either side [1]. Friction between the ballast and the sleepers is further dependent on the normal load on the track, compaction of ballast around the sleepers, and number of ballast particles directly in contact with the sleepers. Normal resistance provided by the ballast to lateral displacement of sleepers at its end is affected by the nature of aggregation of ballast particles at the end of the sleepers and overall ballast gradation.

Figure 2.3 Buckling of railway tracks in the lateral direction due to thermal stresses [10].

Defects in track geometry, both in vertical and in lateral directions, arising due to insufficient support from railway ballast are undesirable because they lead to low traffic speeds, fluctuating wheel-rail contact forces, deterioration of ride quality for passengers, and in extreme cases, derailment. Therefore, correction of such defects is an important component of track maintenance activities for railroads, and has bearing on their operational costs, maintenance routines, passenger ride quality, and safety.

2.1.3 Tamping

Tamping is the process used to restore track settlement by strategically lifting the track where it has settled. This is achieved by mechanically lifting the track and squeezing the surrounding ballast below the raised sleepers. The goal of the tamping process is to attain maximum possible ballast compaction below the sleepers while minimizing damage to ballast particles from the squeezing forces.

Tamping machines, or tampers, traverse on rails which they are lifting and perform tamping of ballast below every sleeper in a repetitive manner. Figure 2.4 shows a tamper in operation [11].

Figure 2.4 A generic representation of a tamper in operation [11].

A single tamping cycle below one sleeper consists of following steps-

1. <u>Lifting of Track</u>

   The tamper lifts the rail track by a calculated height. This height is determined by the required correction in height. A small amount of compensation is included in the calculation to account for initial track settlement after it is dropped back onto the ballast at the end of the cycle. The usual gain achieved in track height by tamping ranges between 20-70mm. A minimum lift of 20mm is often recommended to ensure that enough space is created below the lifted sleepers for ballast particle to be squeezed below them [1]. While

lifting the tracks, the tamper may also correct the lateral track position by compensating for lateral track displacement from its initial position.

2. Insertion of Tamping Tools into the Ballast

   A few pairs of tamping tools, called tines, are inserted into the ballast below the lifted sleepers. Figure 2.5 presents an illustration of the tools and their orientation relative to the sleepers [12].

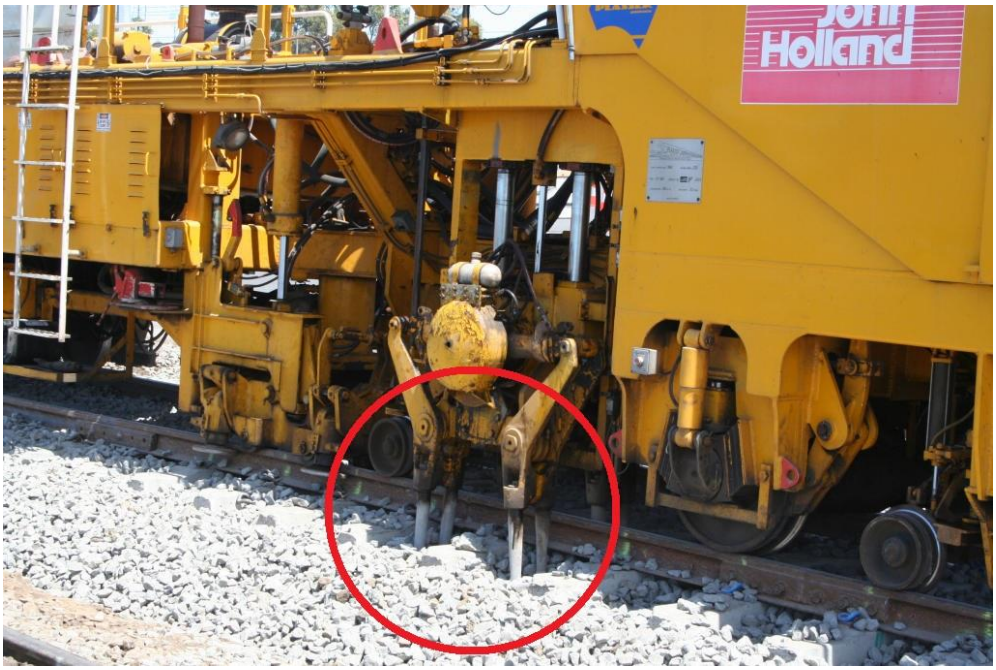

Figure 2.5 A representation of tamping tines being inserted into the ballast [12].

These tines are vibrating throughout the tamping cycle to reduce resistance to their motion from the ballast. Ballast is known to liquefy locally when subjected to vibrating tines, and the higher the frequency of vibration, the more fluid the ballast gets [1]. Consequently, lower frequencies are not able to effectively mobilize the ballast particles and the power requirements of the machine are increased, whereas a stable consolidation of particles below the sleepers cannot be ensured at higher frequencies due to increased mobility of the particles. Parameters of vibration, like frequency, amplitude, and nature of oscillation, vary from manufacturer to manufacturer and are often a point of design conflict. While effect of different vibration behaviors of tines on ballast is well researched, appropriate set of

values of vibration parameters required for minimizing track settlement after tamping is considered ambiguous.

Another design parameters that is critical for achieving optimum results after tamping is the depth of insertion of tamping tines below the sleepers. Exact depth of insertion is dependent on the shape of tines themselves, but the tines are usually inserted until their top edge or face is 10-20mm below the bottom face of the sleepers [1].

3. Squeezing of Ballast below the Sleepers

   As shown in Figure 2.6 below, the tamping tines, once inserted, squeeze the ballast below the lifted sleepers [13].

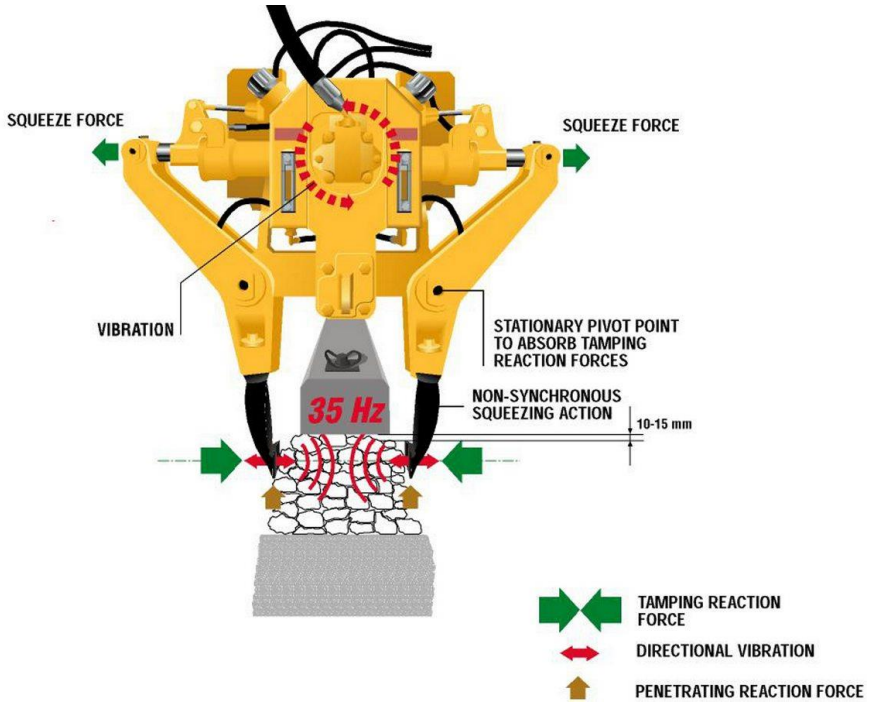

Figure 2.6 Squeezing of ballast below the sleepers by the tamping tines [13].

Tines squeeze ballast with a constant pressure, irrespective of the amount of travel required to attain that pressure. The squeezing action is also non-synchronous in most cases, which means that left and right tines do not necessarily squeeze by the same amount. This has two major advantages. Firstly, voids generated below the lifted sleeper may be of varying sizes, and using constant pressure to squeeze the ballast ensures a certain level of ballast compaction irrespective of the void size. The value of pressure used by various manufacturers, however, is not fixed and normally lies between 100 to 150bar. Secondly,

since the tamper moves along the rail while tamping the sleepers, at any given sleeper being tamped, the previous sleeper is tamped while the next one is not. This implies that the condition of ballast present below the sleeper is not symmetric and non-synchronous action of tines helps mitigate the difference by adjusting the required travel to squeeze the ballast to the same pressure on either side.

The ballast particles, while being squeezed, take a finite amount of time to rearrange themselves below the sleeper [1]. Therefore, the speed of squeezing motion and the amount of time for which the tamping tines hold their position after reaching the squeezing pressure influences the achieved level of compaction. This squeezing hold time usually ranges between 0.8-1.2s.

4. Withdrawal of Tines from the Ballast

   This is the last step of the tamping cycle in which the tamping tines are pulled out of the ballast before the tamper moves to the next sleeper. The velocity of withdrawal of tines influences the loss of compaction that occurs after the withdrawal. While reducing the withdrawal velocity is ideal because it minimizes disturbance to the squeezed ballast, it is unfavorable from the point of view of increasing the overall time taken to tamp a given section of rail track. Therefore, a compromise must be made based on the involved costs.

Tamping can also be used to improve the quality of the rail track to reduce its rate of settlement in the future. The improvement achieved, however, is dependent on the initial track quality before tamping [1]. While the effectiveness of tamping in improving track settlement rates is well established, it is also considered responsible for reducing the lateral track stability by up to 60% [14]. Therefore, the tamping operation is usually followed by other track stabilizing operations such as stone blowing, dynamics track stabilization, etc.

2.2 Discrete Element Modeling (DEM)

Granular systems are disordered aggregates of a large number of particles, characterized by abrupt changes in mass density, anisotropy, non-conservative internal forces, and irreversible deformations of constituent bodies. Traditionally, the behavior of granular assemblies has been modeled using assumptions of continuous mass density and homogeneity. Such modeling

approaches are only suitable for predicting specifically targeted macroscopic parameters of the subject granular assembly for a small range of input conditions. Furthermore, the constants and parameters in models with assumptions of continuity and homogeneity are not indicative of actual physical properties in most cases. Discrete Element Model (DEM) was originally developed by Cundall early 1970s [7], and it has evolved since. DEM takes into account the discontinuous nature of granular systems and allows accurate modeling of both microscopic and macroscopic properties.

The particles in DEM are represented as infinitely rigid bodies that are independent of each other, and interact only when there is contact between any two bodies. The force at the contact is calculated using pre-defined force laws, and the resulting displacement of the particle due to the net contact force is determined in an iterative manner using an explicit time-stepping algorithm. Therefore, DEM calculates the contact dynamics and the kinematics of all particles in the system individually [15].

The DEM package used in this simulation study is PFC^{3D} from ITASCA Consulting Group, Inc. The implementation of the DEM methodology and various components in the PFC^{3D} model have been described in the following subsections-

2.2.1 Walls and Granular Particles

The walls and the granular particles represent the two types of physical bodies whose behavior can be modeled and studied. A collection of small bodies, with well-defined volume and properties, is used to model granular particles. In PFC^{3D}, each particle is defined using either a sphere or an agglomerate of overlapping spheres. Such agglomerates, called clumps, can be used to create arbitrary particle shapes as per requirement, and are treated as a single rigid body [15].

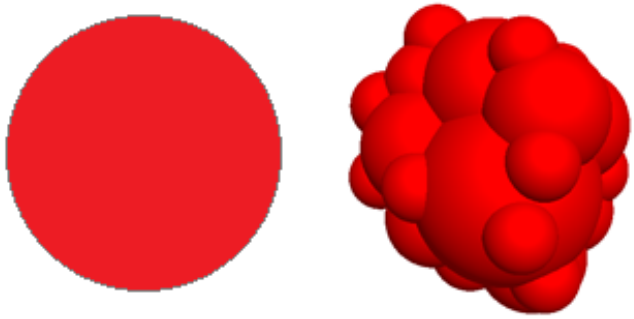

Figure 2.7 A simple spherical particle (left) and an arbitrarily shaped clump (right).

The rigid body assumption for the particles is justified because the macroscopic behavior of a granular assembly is a net result of relative displacement and rotation of all particles, and not of individual particle deformation [15]. PFC^{3D} allows creation of disordered aggregates of large number of particles within a control volume. In the simulation model, the definition of granular particles requires specification of radii in case of spheres, the enclosing surface in case of clumps, and the material properties like mass density, friction coefficient, material damping, shear modulus, etc. by the user.

Walls, on the other hand, represent physical bodies in the simulation environment that apply external forces on the assembly of granular particles, like containers, stirrers, static loads, etc. Walls are user-defined surfaces that are discretized into an arrangement of triangular facets during solution. Definition of wall in the model requires specification of an eligible surface and surface properties like friction coefficient, material stiffness, and damping properties [15]. The kinematics of walls are also completely defined by the user, and thus, walls are not assigned any mass properties.

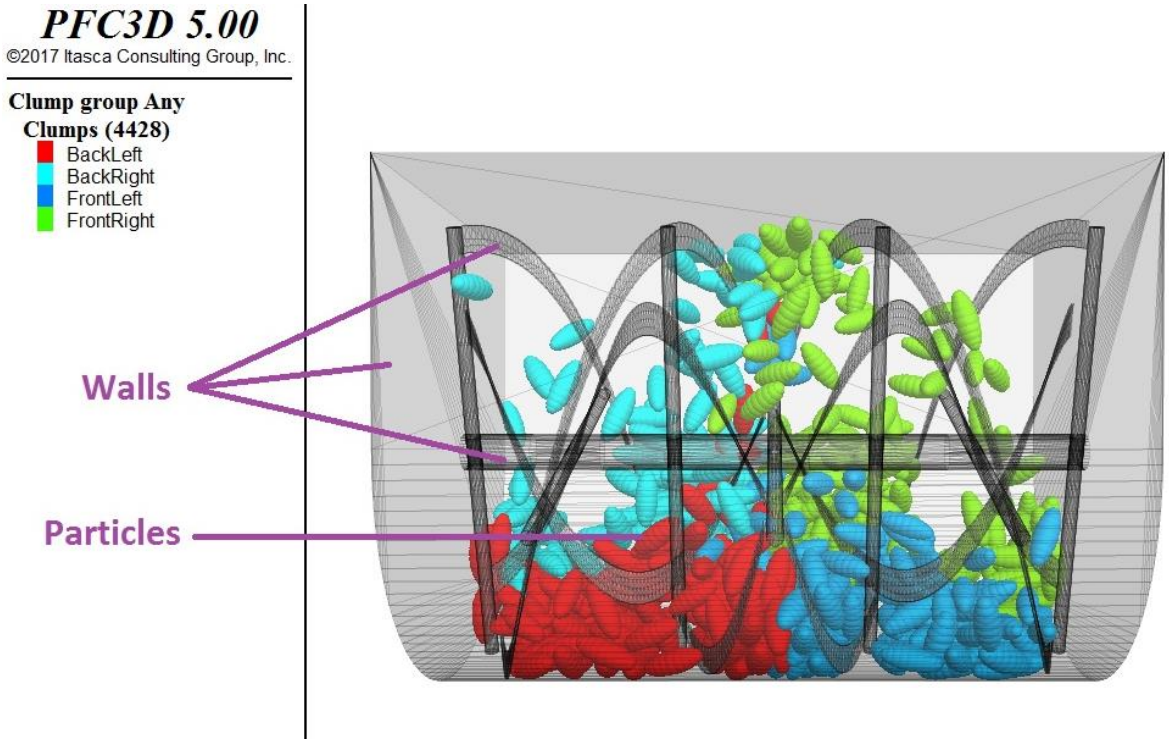

Figure 2.8 An illustration of granular particles and walls in the PFC^{3D} simulation environment [15].

2.2.2 Contact Resolution Between Bodies

Contact detection algorithm includes identification of points of pair-wise contact between all physical bodies in the simulation environment, whether particle-particle or particle-wall. Coordinates of all bodies are tracked throughout the simulation and the contact detection algorithm is applied only on selected physical bodies which are in close proximity to other bodies. Possible contacts are detected by comparing the normal distance between two bodies to their sizes [15].

Once a contact has been detected between two bodies, PFC^{3D} uses a soft-contact approach to model the consequent behavior of the two bodies at the contact point. The soft-contact approach was presented by Cundall and Hart in [16]. In this approach, a small deformation of the bodies is assumed at the contact point for the purpose of calculating the contact force and moment. Since the bodies are also assumed to be perfectly rigid, this deformation is modeled by allowing the two bodies to overlap by a finite amount at the point of contact. The extent of overlap is negligible compared to the size of the bodies. The numerical treatment of this overlap is discussed in the next section.

Since all particles, including clumps, have spherical surface profiles, and can contact other spheres at only one point, particle-particle contact is detected by comparing center to center distance of the spheres to their radii as shown in Figure 2.9a.

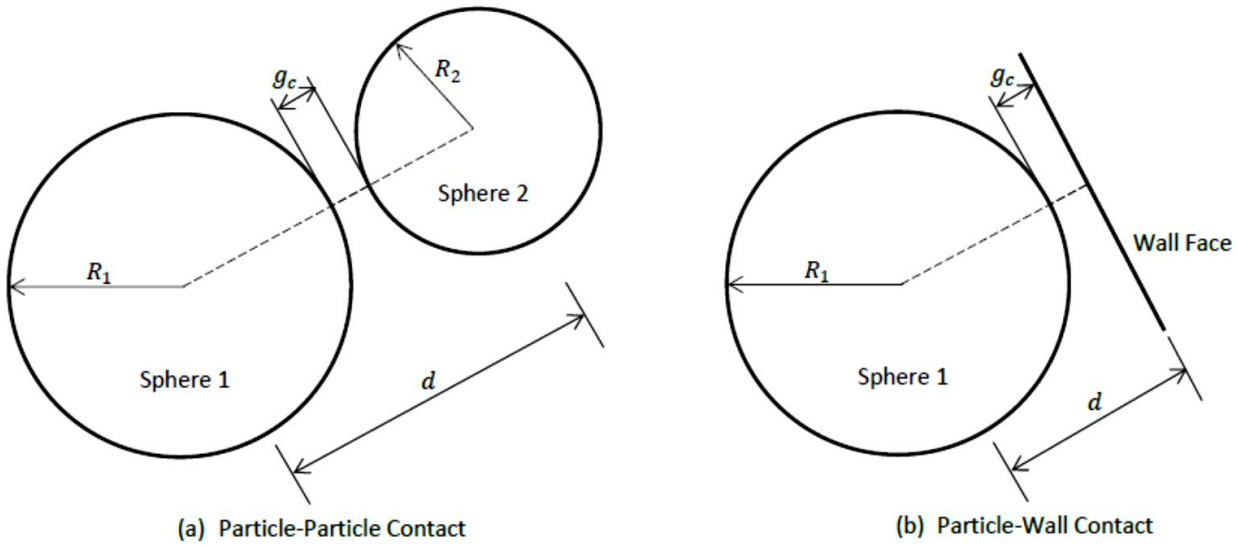

Figure 2.9 Contact detection between (a) particle and particle, and (b) particle and wall

$$g_c = d - (R_1 + R_2) \tag{2.1}$$

Similarly, for the contact between spheres and wall, as shown in Figure 2.9b-

$$g_c = d - R_1 \tag{2.2}$$

If $g_c > 0$, there is no contact between the two bodies

If $g_c \leq 0$, then the bodies are in contact and there is an overlap between them

Where,

g_c	Contact gap between two bodies
R_1, R_2	Radii of the two spheres
d	Distance between the two bodies

As long as any two bodies are in proximity of each other, PFC3D updates the position information for that pair in every cycle of calculation and monitors the contact gap, g_c, to determine the activity state of the contact. If the contact gap becomes negative, the contact is categorized as 'active' and, contact force and contact moment are calculated as described in the following section. Additional considerations are made to ensure that relative motion of the contacting bodies is symmetric about the contact [15].

2.2.3 Calculation of Contact Force and Moments

The overlap at the contact point between two bodies is assigned a calibrated stiffness by the user, and contact force between the two bodies is calculated as a function of the contact gap, g_c, where $g_c < 0$, and the contact stiffness. Damping elements are also modeled at the contact to capture the energy dissipation occurring during collisions between bodies.

$$F_c = f(k, \beta, g_c) \tag{2.3}$$

Where,

F_c	Net contact force
k	Stiffness of the contact
β	Damping of the contact

F_c is the resultant of normal (F_n) and shear (F_s) components of force. Figure 2.10 represents the hypothetical arrangement of springs and dashpots which is used to derive equations for calculation of normal and shear contact forces.

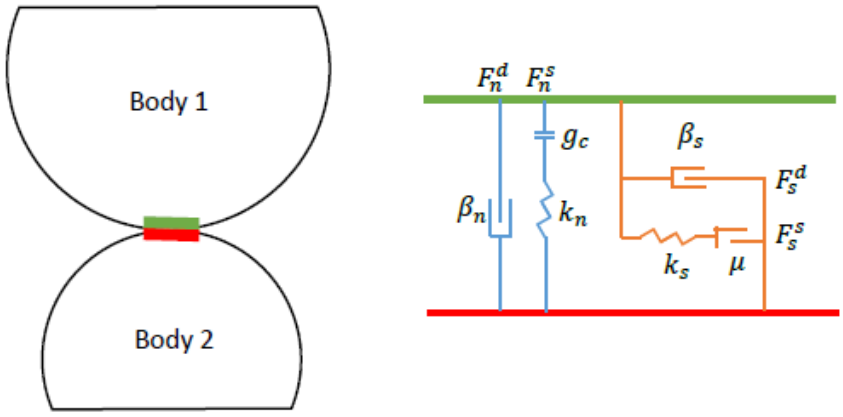

Figure 2.10 General arrangement of forcing and damping components at the contact point [15].

The general formulation of contact force based on this modeling scheme of PFC^{3D} is-

For the normal component,

$$F_n = \underbrace{F_n^s}_{spring\ force} + \underbrace{F_n^d}_{damping\ force} \tag{2.4}$$

Normal spring force, F_n^s, depends on the normal contact stiffness, k_n, and can be linearly or non-linearly dependent on the contact gap, g_c. Normal damping force, F_n^d, is dependent on the damping coefficient, β_n. Element g_s ensures that the normal contact force is applied in compression only.

Similarly, for the shear contact force,

$$F_s = \underbrace{F_s^s}_{spring\ force} + \underbrace{F_s^d}_{damping\ force} \tag{2.5}$$

Spring force in shear, F_s^s, depends on the shear stiffness, k_s, and shear damping force, F_s^d, is dependent on the damping coefficient, β_s. The total magnitude of contact force in shear, F_s, is limited by the maximum available frictional force, as defined by the Coulomb's Law of friction-

$$\max(F_s) = F_s^\mu = -\mu F_n \tag{2.6}$$

The net contact force calculated for a contact point is applied in an equal and opposite sense to the two bodies making the contact. Since for spheres, the contact force passes through the contact point, the contact moment, $M_c = 0$. Therefore, spheres do not resist relative rotation about the point of mutual contact.

The general arrangement of springs and dashpots can also be altered to model more complex granular behaviors, such as, particle fracture, inter-particle adhesive forces, etc. This permits introduction of bonding forces at the points of contact between particles, and the spring forces to act in tension until they reach a specified maximum value, after which the bond breaks and the two particles separate. In such cases, contact moment, M_c, may not always be zero [15].

The exact numerical expressions for calculating spring and damping force components, both in normal and in shear, are defined by the contact-displacement law chosen by the user. This law is also referred to as the Contact Model. Different contact models are suitable for different types of physical systems, and have a bearing on accuracy and validity of the solution. PFC^{3D} offers nine pre-defined contact models, including the ones that are most commonly used. Selection of an appropriate contact model for modeling of railway ballast particles will be discussed in the following chapters.

2.2.4 Particle Trajectories and the Time Stepping Algorithm

The trajectories of all particles by virtue of being acted upon by contact forces are calculated by applying Newton's laws of motion on the bodies. The motion of walls is defined by the user and is unaffected by the contact forces acting on the wall.

The solution scheme employs an explicit time stepping algorithm for repetitive application of Newton's laws based on updated contact force data. The simulation advances in time by performing a series of calculations and logical operations in a sequential manner. The solution algorithm used by PFC^{3D} is shown in Figure 2.11.

The time-step calculation is based on constraints placed by displacement rates of bodies and their contact stiffness, and the minimum time-step is chosen for that cycle. The size of the time-step is such that particle velocities and accelerations are assumed to be constant within that time instant. This implies that, in one time-step, any disturbance can propagate from one particle to its

immediate neighbors only and all forces acting on a particle are exclusively due to its contact with other bodies during that time-step.

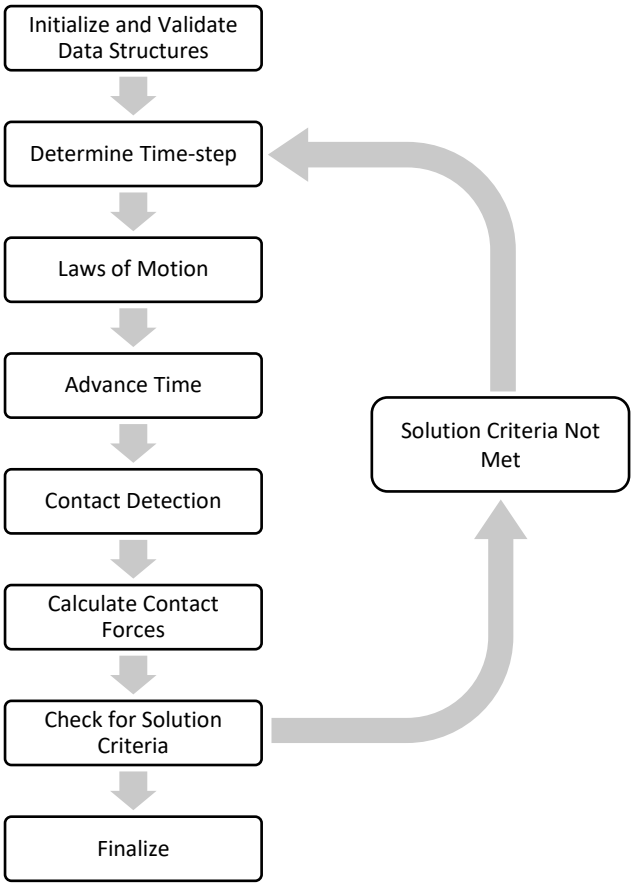

Figure 2.11 The sequence of operations in one calculation cycle of PFC^{3D}.

2.3 Applicability of DEM for Studying Railway Ballast Behavior

Since its development in the early 1970s, DEM has been widely adopted as a primary modeling and simulation tool for granular aggregates in the fields of geomechanics, rock mechanics, soil mechanics, manufacturing and packaging industry, and even astronomy. Because of its granular nature, railway ballast also yields itself to investigation using DEM methods. Multiple researchers have employed various DEM techniques to study the behavior of railway ballast from a diverse number of perspectives. These include study of its mechanical behavior, mesoscopic and macroscopic dynamics, particle kinematics, loading behavior, and particle breakage.

Discrete Element Models of railway ballast have been presented in the literature by Tutumluer [17, 18], Lu [19], Gonźalez [20], Cholet [21], Stahl [22], and Indraratna [23] among many others.

Response of railway ballast to standardized loading conditions like monotonic loading, triaxial loading, cyclic triaxial loading, and direct shear loading has been simulated using DEM by Saussine et al. [24], Indraratna et al. [25], and McDowell et al. [26, 27] with encouraging levels of accuracy.

Mechanical behavior of railway ballast due to cyclic loading from rail traffic has also been explored using DEM. McDowell and Lim conducted a famous ballast box experiment to record track settlement data due to traffic loading and replicated the results using DEM simulations [28, 29]. Indraratna et al. also simulated cyclic loading on ballast and validated it using experimental data [30]. Vallejo et al. studied the response of railway ballast to cyclic traffic loading in [31].

One of the most prominent areas of interest regarding research in railway ballast is the change in properties of ballast due to variations in shape and size distribution (gradation) of its constituent particles. Tutumluer at. al. have presented pioneering analysis on effects of ballast gradation on track stability, tamping, aggregate packing, and overall ballast performance [14, 32, 33]. McDowell et al. emphasized on the significance of correctly modeling particle shapes in DEM simulations in [34] by highlighting the differences in ballast behavior for different particle shapes subjected to identical loading conditions.

A modest amount of literature is also available on modeling of railway ballast for the study of tamping operation using DEM. Zhou et al. have shown the changes in mechanical properties of ballast and inter-particle contact forces during tamping for a range of tine frequencies and amplitudes [35-37]. Radjai et al. and Saussine et al. have also conducted parametric studies of the tamping process to study ballast compaction and optimization using DEM [38-41]. A discrete element model of the railroad tamping process has also been presented by Wang et al. [42].

Apart from the research mentioned above, DEM has sporadically been employed to model degradation and fouling of ballast particles during service [23, 43, 44], comparison of ballast compaction by different maintenance methods [45], comparison of sleeper designs [46], and even for the development of instrumented and engineered ballast.

Based on the above, DEM is evidently a versatile tool for simulating granular systems and its application for furthering scientific understanding of the properties and behavior of railway ballast

is indisputable. However, as described in the next section, utilization of DEM for modeling railway ballast is subject to certain practical considerations and challenges.

2.4 Challenges to Modeling of Railway Ballast Using DEM

Fidelity and feasibility of DEM simulations is contingent on the following considerations regarding calibration of modeling parameters, validation of results of the simulation, and numeric execution of the model-

1. DEM of railway ballast is computationally intensive

Computational requirements of a DEM simulation are primarily governed by-

- number of bodies in the simulation model,
- complexity of particle shape,
- number of pair-wise contacts that are required to be detected and resolved, and
- magnitude of kinematic acceleration of the moving bodies.

All of these factors act unfavorably in case of railway ballast particles. A ballast aggregate, especially in a tamping model, constitutes a large number of randomly shaped particles with a wide range of sizes. This implies that there are a large number of particles with complicated shape and size distribution, and they have large number of contacts amongst them. Additionally, since ballast particles are extremely stiff and rigid, large accelerations occur due to steep changes in contact forces. Large accelerations, consequently, warrant smaller simulation time-steps for effectively capturing all particle dynamics. Therefore, computational times for railway ballast simulations can be of order of several weeks depending on the model and the available computing hardware.

2. Calibration of contact physics is complicated

Definition of any contact model between a pair of bodies requires independent specification of contact stiffness for both bodies, damping coefficients at contact points, local damping of the bodies, and friction coefficient for the pair of bodies. For most contact models, these parameters,

except the friction coefficient, are numerical artifacts and have no real physical significance. Values of these parameters is calibrated á posteriori from the comparison of simulation results with experimental results, often based on overall collision time between two bodies and their coefficient of restitution [47-50]. Furthermore, parameters like damping, which affect the rate and the nature of energy dissipation within the assembly, cannot be measured by experimentation. Modeling of contact force laws between a pair of bodies is an area of ongoing scientific research, and despite presence of anomalies in such contact models, overall macroscopic behavior of the granular assemblies can be reliably captured and studied.

3. Experimental validation of simulation results is difficult

The experimental validation of results of DEM simulation is onerous for several reasons. Firstly, accurate calibration of contact model in the simulation requires extensive experimentation to study contact forces between bodies as a function of microscopic deformations of the contacting bodies during the collision. Secondly, physical measurement of the output variables of a DEM simulation, such as particle compaction, inter-particle contact forces, number and distribution of contacts in the assembly, etc., is not pragmatic, especially for railway ballast. Therefore, additional simulations or experimentation might be required to study and compare practically observable effects of such fundamental output variables. Lastly, granular systems are random, disordered, and chaotic. For example, it has been shown that two identical rail tracks with identical ballast gradations and subsoil do not settle at the same rate when subjected to identical loading conditions [8]. A DEM simulation, therefore, only computes one of many possible solutions for a particular granular assembly. Relatively varying results could be obtained every time a simulation or an experiment is performed and fidelity of modeled physical behavior, thus, cannot be assured [47].

3. Modeling of Contact Physics

Modeling of contact physics entails determination of several model parameters that dictate forces between two colliding bodies. These forces include spring, damping, and frictional forces in the normal and the tangential direction at a contact point. This chapter deals with the rationale behind selection of appropriate contact model and calculation of all forces acting at contact points.

3.1 Comparison of the Contact Models

Contact models consist of the force displacement law, which expresses the contact force as a function of the overlap at the contact point, g_c. PFC^{3D} offers nine built in contact models-

1. Linear
2. Linear Contact Bond
3. Linear Parallel Bond
4. Hertz
5. Hysteretic
6. Smooth Joint
7. Flat Joint
8. Rolling Resistance Linear
9. Burger's

Each of these models is suitable for a different type of application and focus on different aspects of granular behavior. Linear contact model, Linear Contact Bond Model, Rolling Resistance Linear Model, and the Hertz contact model have been found suited for the analysis of dense granular systems and are most frequently used to model railway ballast.

3.1.1 Linear Contact Model

As expressed by equations 2.3, 2.4, and 2.5 in the previous chapter, a contact model has a spring force component and a damping (dashpot) force component. Both components exist in normal as well as shear directions, and in the case of a Linear model, are calculated as follows-

Normal linear spring force, F_n^l

$$F_n^l = \begin{cases} k_n g_c, & g_c < 0 \\ 0, & otherwise \end{cases} \tag{3.1}$$

where, k_n is the normal contact spring stiffness.

Shear linear spring force, F_s^l

F_s^l is computed in an incremental manner by a multistep procedure. First, a trial shear force, F_s^*, is calculated as:

$$F_s^* = F_s^l|_0 - k_s \Delta\delta_s \tag{3.2}$$

Where,

$F_s^l|_0$ is the shear force at the beginning of the time-step,

k_s is the shear contact spring stiffness, and

$\Delta\delta_s$ is the incremental shear displacement during the time-step.

The shear strength of the contact, F_s^μ, is determined by the limit of Coulomb's friction.

$$F_s^\mu = -\mu F_n^l \tag{3.3}$$

Finally, the shear contact force, F_s^l, is calculated as-

$$F_s^l = \begin{cases} F_s^*, & \|F_s^*\| \le F_s^\mu \\ F_s^\mu \left(\frac{F_s^*}{\|F_s^*\|}\right), & otherwise \end{cases} \tag{3.4}$$

And the slip rate, s, is updated to set the sliding status of the contact.

$$s = \begin{cases} true\ (sliding), & \|F_s^l\| = F_s^\mu \\ false\ (not\ sliding), & otherwise \end{cases} \tag{3.5}$$

Normal damping force, F_n^d

$$F_n^d = \left(2\beta_n\sqrt{m_c k_n}\right)\dot{\delta}_n \tag{3.6}$$

Where,

β_n is the normal damping coefficient,

$\dot{\delta}_n$ is the relative normal translational velocity, and

m_c is the equivalent mass of the contact, and is calculated as-

$$m_c = \begin{cases} \dfrac{m_1 m_2}{m_1 + m_2}, & particle - particle\ contact \\ m_1, & particle - wall\ contact \end{cases} \tag{3.7}$$

m_1 and m_2 are the masses of both particles in contact respectively.

Shear damping force, F_s^d

$$F_s^d = \begin{cases} \left(2\beta_s\sqrt{m_c k_s}\right)\dot{\delta}_s, & s = false \\ 0, & s = true \end{cases} \tag{3.8}$$

Where,

β_s is the shear damping coefficient, and

$\dot{\delta}_s$ is the relative shear translational velocity.

3.1.2 Linear Contact Bond Model

A contact bond assigns a finite tensile and shear strength to the point of contact such that small tensile forces are possible. Further, the shear force is limited by the assigned shear strength instead of the Coulomb's friction. If external forces exceed the bond strength in any direction, the bond is broken, and the contact status is changed to unbonded. After the contact changes to unbonded, normal Linear model formulation is imposed. The tensile and the shear strengths of the bonds are specified by the user.

Based on Figure 2.10 from the previous chapter, the modified spring dashpot schematic with contact bonds is shown in Figure 3.1.

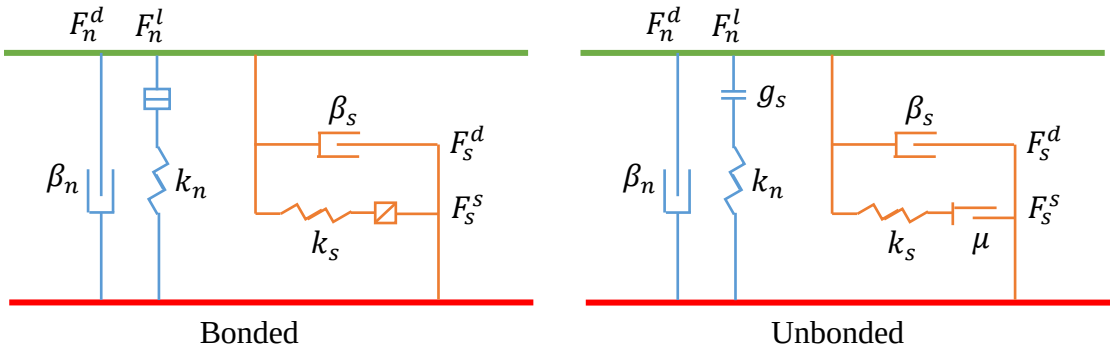

Figure 3.1 Modified spring-dashpot layout schematic for a Linear model with a contact bond.

The normal linear spring force formulation changes as shown-

$$F_n^l = \begin{cases} \begin{cases} k_n g_c, & g_c < 0 \\ 0, & otherwise \end{cases}, & unbonded \\ k_n g_c, & bonded \end{cases} \tag{3.9}$$

3.1.3 Rolling Resistance Linear Model

No moment is applied at the contact point between two spheres by default. Therefore, two spheres in contact can rotate freely about each other. This rolling behavior is unrealistic in case of ballast particles and is compensated by applying an artificial moment at the contact point to resist relative rotation of contacting particles. This moment increases proportionally to the accumulated relative rotation between the particles and is cut off at a limiting value.

The contact moment, M_c, is calculated in an incremental manner as-

$$M_c \coloneqq M_c - k_r \Delta\theta_b \tag{3.10}$$

$$k_r = k_s \overline{R}^2 \tag{3.11}$$

$$\frac{1}{\overline{R}} = \frac{1}{R_1} + \frac{1}{R_2} \tag{3.12}$$

Where,

k_r is the rolling resistance stiffness,

$\overline{R}$ is the contact effective radius,

R_1 and R_2 are the radii of two particles in contact. For walls, $R_2 = \infty$.

The limiting torque, M^*, is defined as-

$$M^* = \mu_r \overline{R} F_n^l \tag{3.13}$$

And then,

$$M_c = \begin{cases} M_c, & \|M_c\| \le M^* \\ M^* \left(\frac{M_c}{\|M_c\|}\right), & otherwise \end{cases} \tag{3.14}$$

Finally, the rolling slip state is also update similarly to the sliding state.

$$s_r = \begin{cases} true\ (rolling), & \|M_c\| = M^* \\ false\ (not\ rolling), & otherwise \end{cases} \tag{3.15}$$

3.1.4 Hertz Contact Model

The formulation of all force components in the Hertz contact model is as:

Normal Hertz spring force, F_n^h

$$F_n^h = \begin{cases} -h_n |g_c|^\alpha, & g_c < 0 \\ 0, & otherwise \end{cases} \tag{3.16}$$

$$h_n = \frac{2\bar{G}\sqrt{2\bar{R}}}{3(1-\bar{\nu})} \tag{3.17}$$

$$\bar{G} = \frac{G_1 + G_2}{2} \tag{3.18}$$

$$\bar{\nu} = \frac{\nu_1 + \nu_2}{2} \tag{3.19}$$

$$\frac{1}{\bar{R}} = \frac{1}{2}\left(\frac{1}{R_1} + \frac{1}{R_2}\right) \tag{3.20}$$

Where,

α is the model exponent,

h_n is the normal Hertzian contact stiffness,

G_1 and G_2 are the shear moduli of the two bodies in contact,

ν_1 and ν_2 are the Poisson's ratios of the two bodies in contact, and

R_1 and R_2 are the radii of the two particles in contact.

For a wall, $R_2 = \infty$

Shear linear spring force, F_s^h

F_s^h is computed in an incremental manner by a multistep procedure. First, a trial shear force, F_s^*, is calculated as:

$$F_s^* = F_s^h|_0 + h_s \Delta\delta_s \tag{3.21}$$

$$h_s = \frac{2(1-\nu)}{2-\nu} \alpha h_n (F_n^h)^{\frac{\alpha-1}{\alpha}} \tag{3.22}$$

Where,

$F_s^h|_0$ is the shear force at the beginning of the time-step,

h_s is the shear contact stiffness, and

$\Delta\delta_s$ is the incremental shear displacement during the time-step.

The shear strength of the contact, F_s^μ, is determined by the limit of Coulomb's friction.

$$F_s^\mu = -\mu F_n^h \tag{3.23}$$

Finally, the shear contact force, F_s^l, is calculated as-

$$F_s^h = \begin{cases} F_s^*, & \|F_s^*\| \le F_s^\mu \\ F_s^\mu \left(\frac{F_s^*}{\|F_s^*\|}\right), & otherwise \end{cases} \tag{3.24}$$

And the slip rate, s, is updated to set the sliding status of the contact.

$$s = \begin{cases} true\ (sliding), & \|F_s^h\| = F_s^\mu \\ false\ (not\ sliding), & otherwise \end{cases} \tag{3.25}$$

Normal damping force, F_n^d

$$F_n^d = \left(2\beta_n\sqrt{m_c k_n}\right)\dot{\delta}_n \tag{3.6}$$

$$k_n = \alpha h_n \delta_n^{\alpha-1} \tag{3.26}$$

Where,

k_n is the normal tangent stiffness,

$\dot{\delta}_n$ is the relative normal translational velocity, and

m_c is the equivalent mass of the contact.

Shear damping force, F_s^d

$$F_s^d = \begin{cases} \left(2\beta_s\sqrt{m_c k_s}\right)\dot{\delta}_s, & s = false \\ 0, & s = true \end{cases} \tag{3.8}$$

Where,

β_s is the shear damping coefficient, and

$\dot{\delta}_s$ is the relative shear translational velocity.

3.2 Selection of Appropriate Contact Model

There are crucial differences in performance and practicality of the Linear and the Hertz contact force models. Performance and accuracy of a contact model is often judged by validation of coefficient of restitution and duration of collision for the pair of bodies in contact. Coefficient of restitution is the ratio of relative velocity of particle after collision to their relative velocity before collision. It is a measure of elasticity of the collision and matching it to experimental measurements is a common way of validating contact models. A relatively less conventional parameter of evaluating the accuracy of a contact model is the duration of collision. Stevens and Hrenya experimentally validated various contact models and compared their accuracy using a set-up to measure coefficient of restitution and collision duration for a pair of colliding spheres [50]. Results

presented by their study reveal that Hertzian contact model is closer to experimentally observed behavior than the Linear model. Hertzian model predicts the collision time to be within 10% of experimental values but none of these models have realistic trends for coefficient of restitution. The contact force versus overlap behavior for the Hertzian model was also more accurate than that of the Linear model.

Lim and McDowell also validated their DEM for railway ballast using three different experimental methods and concluded that Hertzian contact model will be more suitable than a Linear model in predicting variability in contact stiffness of ballast particles due to changing contact forces [28]. Goldsmit [51] also established that Hertzian model is well suited for sphere-sphere and sphere-wall contacts if materials are highly stiff and impact velocities are small, such as for railway ballast.

Additionally, the stiffness constants in the Linear model, k_n and k_s, do not correspond to any real physical quantity and can only be heuristically established by ensuring that simulation results agree with the experimental observations. Fidelity of these parameters thus, can only be assessed à posteriori, after analyzing the results from the simulations and there is no way of estimating their value beforehand [47]. On the other hand, stiffness constants in the Hertz model, h_n and h_s, can be derived from the material properties of the bodies in contact as shown in equations 3.17 and 3.22.

Therefore, since Hertz model allows more accurate recreation of the physical contact behavior, and its parameters are more practically feasible to determine, Hertz model was chosen for contact modelling of railway ballast. The choice of contact model has no significant effect on the overall computational time of the simulation [47].

3.3 Configuration of Contact Model Parameters

Numerous material and physical properties need specification for complete and valid configuration of Hertz contact model within the simulation. These properties will be discussed next.

Mass Density

Mass density needs specification for spheres but not for walls. Mass density is used for individual calculation of masses of all particles in the simulation environment, which in turn determines the gravitational and contact forces acting on them. For ballast particles made of basalt, a mass density of $2750\ kg/m^3$ is used.

Poisson's Ratio

Poisson's ratio is used for calculation of contact forces by the Hertz contact model, and needs to be specified for both particles and wall entities. It is set as 0.2 for ballast particles made of basalt, and as 0.3 for wall entities (tines) made of steel. All walls in the simulation must have identical contact parameters.

Shear Moduli

Shear modulus is required for particles and walls for calculation by Hertz model. Both ballast particles and walls are assumed to be made of homogenous and isotropic materials, and therefore, their shear modulus, G, can be expressed as-

$$G = \frac{E}{2(1+\nu)} \tag{3.27}$$

Where, E is the Young's modulus of the material and ν is the Poisson's Ratio.

Since Poisson's ratios for both particles and walls are already specified, only Young's moduli need definition. The Young's modulus for basalt is set to be 50GPa and 200GPa for steel.

Friction Coefficient

As described in the previous section, friction coefficient determines the maximum available shear force at the contact points between bodies. Although friction coefficient between ballast particles can vary between 0.48 and 0.7 [52], it is set to be 0.6 for both particle-particle and particle-wall interfaces. Abbaspour-Fard [53] asserted that frictional behavior of the clumps changes depending on packaging of the constituent spheres of the clump and argued for modification of friction

coefficient to compensate for its influence. Investigation of the effects of spherical packaging within individual clumps on the frictional behavior of particles lies outside the scope of this project but needs to be undertaken in a future study.

Damping Coefficients

PFC3D allows configuration of two types of damping coefficients- viscous (β_n and β_s) and local (β_l). Viscous damping occurs at contact points between bodies due to presence of normal and shear dashpots at the contact. This damping is proportional to the relative velocities of the two bodies during collision. Alternatively, local damping acts on each particle individually and is proportional to the magnitude of unbalanced force acting on the particle. Values of these damping coefficients determine the rate of dissipation of energy in the granular assembly as well as the primary mode by which the energy is lost. PFC3D provides guidelines of setting ballpark values of these coefficients in different scenarios and recommends setting local damping to a lower value than the viscous damping for dynamic simulation of highly compacted assemblies such as railway ballast [15]. Based on the empirically derived information available in the literature, viscous damping for particle-particle contacts is set at 0.8, and at 0.6 for particle-wall contacts. Local damping for particles is set at 0.6 as well.

4. Modeling of Ballast Gradations

The initial step in modeling railway ballast in PFC^{3D} is specification of ballast gradation and generation of particles in the simulation environment per the gradation. Specification of ballast gradation includes description of particle shapes and declaration of size distribution of particles in the granular assembly. As mentioned in the previous chapter, particles can either be modeled as spheres or clumps. The method of specification of ballast gradation in the simulation is dependent on the type of particle shape selected.

4.1 Modeling Ballast Particles as Spheres

When modeling ballast particles as spheres, the shape information of the particles is discarded, whereas the size information is captured by specifying the radii of modeled spheres. The size of a particle is defined as the minimum sized mesh through which it can pass. In the simplest case, all spheres in the model have equal radius and size distribution information is not required. In the case of a collection of spheres of varying radii, the size distribution of spheres must be similar to the size distribution of the sample of ballast being modeled. By using pre-defined distributions within the software, such as Gaussian, or by defining custom functions within the script, any given size distribution can be recreated by the user in PFC^{3D}.

4.2 Modeling Ballast Particles as Clumps

If ballast particles are modeled as clumps, unlike spheres, their shape information is preserved. As shown in Figure 4.1, PFC^{3D} accepts the 3D scanned surface profiles of stones to be modeled in *"stl"* format and then generates clump templates. A clump template is a fixed arrangement of overlapping spheres of varying radii corresponding to the three-dimensional surface profile of any particle. A clump, despite being made of constituting spheres, is treated as a single rigid body.

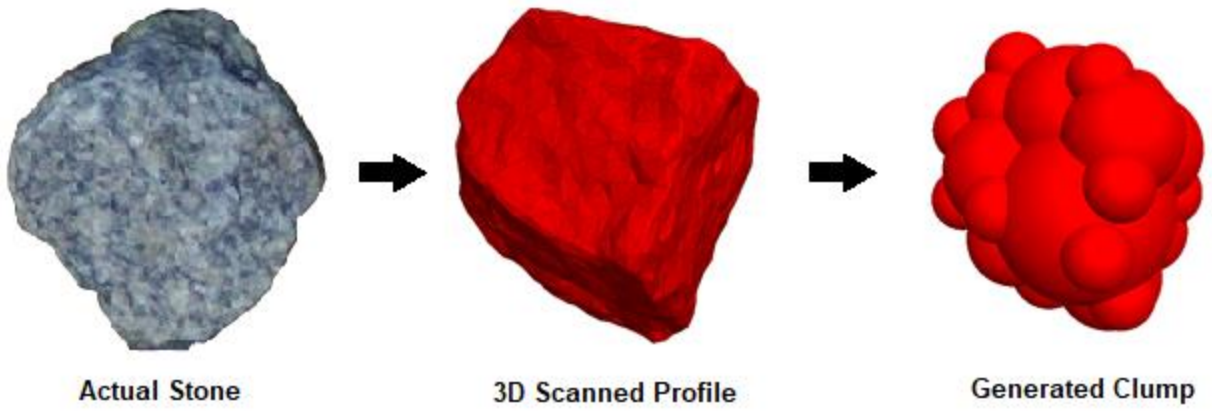

Figure 4.1 Defining clumps to model railway ballast particles.

The arrangement and sizes of the spheres in the clump template is determined by the Bubble Pack algorithm in PFC^{3D}. This algorithm allows the user to manipulate the number of spheres used to create the template, as well as the radii and the locations of these spheres, therefore, allowing full control of the level of detail of the surface profile captured for the purpose of modeling. Figure 4.2 shows the difference in the level of surface detail captured by changing clump generation parameters within the simulation script.

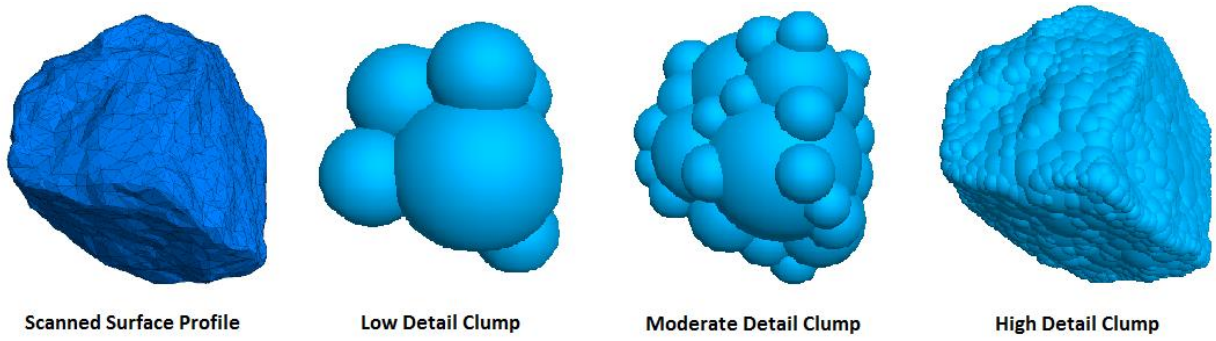

Figure 4.2 Controlling surface detail of the particle by manipulating clump generation parameters.

Increasing surface detail of the clumps increases computational requirements of the simulation as well. Arrangement of spheres within the clump also has a bearing on their mechanical response. Frictional properties and the collision behavior of the clumps is affected by the size and the density of their constituent spheres [53]. A complete ballast gradation consisting of a number of such irregularly shaped clumps can be replicated in the simulation environment by individually

importing the surface profiles of stones from a sample of the ballast, and specifying the absolute number or the percentage (of total number) of particles having that shape. Calibration of clump generation parameters will be considered in depth in the future based on accuracy and fidelity requirements of results of the tamping study.

An alternative way of capturing the particle shape in DEM simulation is by representing modeled particles as a polyhedral closed surface made of small planar elements. Figure 4.3 shows a few examples of such polyhedral closed surfaces. The resolution of detail of the surface of the particle is controlled by adjusting the size and the number of small planar elements in the polyhedron.

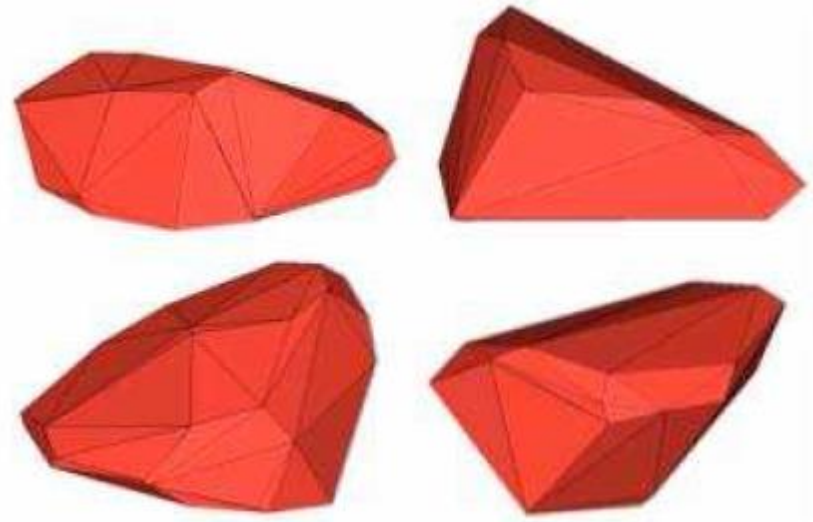

Figure 4.3 Examples of polyhedrons used for representing ballast particles [54].

Modeling particles as clumps offers some crucial advantages over modeling as polyhedrons. Firstly, as covered in Chapter 2, every contact is ultimately a contact between two spheres in the case of clumps, contact detection and resolution within the solution algorithm is much simpler than that for polyhedrons. Complexities can arise in contact detection for a pair of non-convex or highly angular polyhedrons due to possibilities of multi-point contact and through penetration during modeling of overlap at the contact [55]. As shown in Figure 4.4, two angular polyhedrons can intersect each other at their sharp edges and vertices, complicating the contact resolution and increasing the solution time.

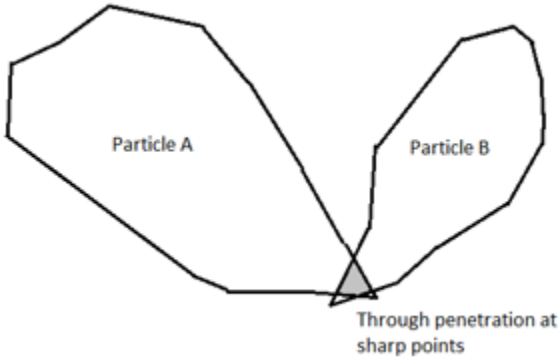

Figure 4.4 Examples of complicated contact resolution for a pair of sharp polyhedrons.

Secondly, since clumps are composed of smaller constituent spheres and not made of a unified entity like a polyhedron, particle breakage and crushing can be modeled by specifying the bond strength between constituent spheres and allowing them to separate under special circumstances. Detailed explanation of this methodology lies behind the scope of this thesis, but for the reasons of versatility, and future expandability of the model, clumps are chosen as the adopted approach of modeling particle shapes.

4.3 Comparison of Particle Shapes

As described previously, spheres and irregular are the two particle shapes that can be used to model railway ballast stones in DEM simulations. Selection of a particle shape out of the two is dependent on the goals of the study and is crucial for obtaining reliable results from the model. Apart from determining the quality and credibility of the results, shape selection also determines the time taken to completely solve the simulations.

Spherical particles are computationally economical and contact physics for them is easier to calibrate. This makes them appealing for undertaking preparatory studies for understanding gross mechanical behavior of ballast systems. Lobo-Guerrero and Vallejo presented a two-dimensional simulation study using circular discs, in which they analyzed crushing of ballast particles due to cyclic loading from rail traffic [31]. While experimental validation of the simulation results was not discussed, they acknowledged that the approximation of particle shape as discs was a potential source of error in their results. González studied lateral track stability using railway ballast

modeled as an aggregate of spherical particles [20]. He modeled artificial rolling resistance at the contact points between the spherical particles to compensate for interlocking between angular ballast particles and claimed to obtain experimentally accurate results. Dynamic behavior of rail track structure was also studied under loading by approximating ballast as a lattice of identical spheres by Ricci et al. [56]. Ricci used a hybrid continuum model with discontinuities in the railway ballast being accounted for by representing ballast as a three-dimensional lattice of discrete spheres.

Clumps have also been widely used to model ballast particles. Sophisticated ballast behavior such as mechanical behavior under loading, particle breakage, effect of ballast gradations, ballast fouling, track stability, and behavior during tamping has been studied and validated using clumps by researchers like McDowell [19, 26, 27, 29, 34, 46] and Indraratna [23, 25, 30, 43]. Similar studies have also been undertaken using polyhedral representations of ballast particles by Tutumluer et al. [14, 17, 18, 32, 33] and Radjai et al. [38-41, 54].

According to these studies, while clumps (and polyhedrons) are definitely effective in reproducing complex ballast response for a variety of input conditions, ballast models employing spherical particles with enhanced inter-particle contact physics can also reliably predict gross ballast performance at a fraction of the computational cost of the former. Although, a few dispersed articles in literature highlight crucial differences in the behavior of spherical and clump ballast particles. Rounded particles have been proved to be have lower shear strength and absence of inter-particle interlocking compared to more angular particles. Consequently, ballast composed of spherical particles will have high track settlement rates and low stability under loading from traffic [32]. Lim compared the behavior of spherical particles to that of clumps under traffic loading, and validated it using physical experimentation through his Ballast Box test [28]. He showed that displacement and load distribution behavior of spherical particles was unrealistic, whereas clumps behaved similar to the ballast in his experimental setup. He also emphasized the absence of inter-locking between spherical particles. Lu suggested that this difference in behavior of spheres and clumps can be bridged by adding artificial rolling resistance and weak bonding forces at the inter-particle contact points [34]. However, such artificial forces have been criticized by others for making DEM simulations inconsistent with the concepts of classical mechanics and possibly introducing unanticipated anomalies in the mesoscopic behavior of granular systems [55].

4.4 Selection of Appropriate Particle Shape for Modeling

A simulation study was conducted to analyze the anomalies presented by use of simple spherical particles for representing railway ballast in DEM studies. Different particle shapes with varying gradations, as listed below, were selected for comparison-

- Identical Spheres- All particles in the simulation are spheres of diameter 40mm.
- Assorted Spheres- Radii of 10% of the total number of spheres have Gaussian distribution in the range 20- 36mm. Another 80% have their radii with Gaussian distribution between 36mm and 44mm. And lastly, radii of the remaining 10% have Gaussian distribution between 44mm and 70mm.
- Identical Irregular- The granular assembly is made of an aggregate of identical clumps which represent an actual arbitrarily shaped ballast particle, roughly the same size as a sphere with 40mm diameter.
- Assorted Irregular- A randomly selected sample of 17 arbitrarily shaped ballast stones of varying sizes was modeled as clumps. This case represents the most realistic ballast gradation.

In all four test cases, 4300 ballast particles were simulated, and output parameters directly related to performance of ballast during tamping were recorded and compared. These parameters are:

1. Ballast Compaction- It is represented as the solid fraction, i.e., the percentage of total volume occupied by solid mass of ballast particles. High compaction below sleepers increases track stability and results in low track settlement rates.
2. Coordination Number- It is the average number of contacts which every particle in the system has with its immediate neighbors. The higher the coordination number of ballast particles, the better the interlocking among particles, and lower the load transmitted per contact. Therefore, high coordination number leads to high track stability.
3. Absolute Number of Contacts- It is the total number of pairwise contacts between all physical bodies within the system (except between two wall entities). In most cases, the coordination number and the absolute number of contacts are positively correlated. Large number of contacts between ballast particles and a sleeper, for example, indicate high frictional forces on the sleeper in the lateral direction, and therefore, high lateral track stability.

4. Load Paths- It is a graphical illustration of the way external and internal forces are transmitted or dispersed through the bulk of the granular aggregate.
5. Vertical Contact Force on Tamping Tines- This is the net resistance which the ballast offers to penetration by tamping tines during the insertion phase of tamping. High resistance would increase the power requirements of the tamping equipment.
6. Simulation Time- It is the total time taken by one simulation run to reach complete solution. This parameter, although does not affect the results of the simulation, is a crucial factor in establishing practicality of simulations employing a particular particle shape.

4.4.1 Design of Simulation Study

To compare the performance of different particle shapes based on the aforementioned parameters, a simulation study was designed. 4300 particles were randomly generated and were made to settle naturally under gravity in an identical cylindrical container in all cases. Later, as shown in Figure 4.5, the naturally settled heap was compacted by applying a static load of 25kg at the top of the heap and the output parameters were recorded. During the compaction phase, inter-particle friction was set to zero to facilitate maximum possible compaction. A static load of 25kg was selected because higher loads would induce larger dynamics in the ballast, thereby reducing the timestep during calculation cycles and increasing the simulation time.

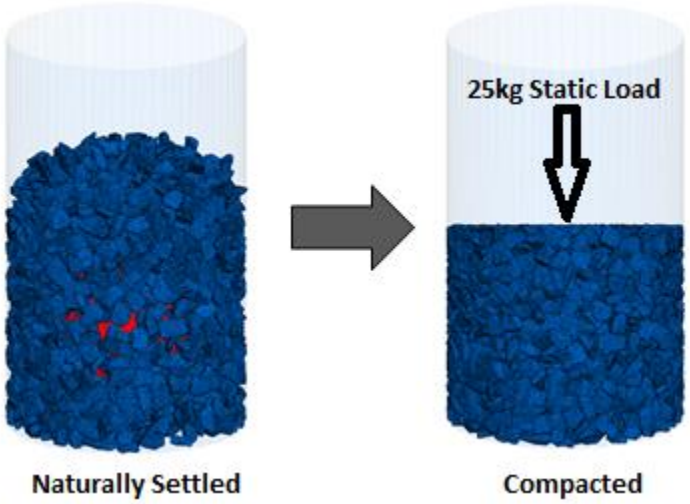

Figure 4.5 Compaction of ballast particles in the simulation study.

For the comparison of vertical contact force on tamping tines, a tamping tool vibrating at 45Hz about its vertical axis was inserted into the ballast unto a depth of 0.5m at a constant velocity of 0.5m/s. During the penetration, the net vertical contact force acting on the tool was recorded for its entire duration of motion.

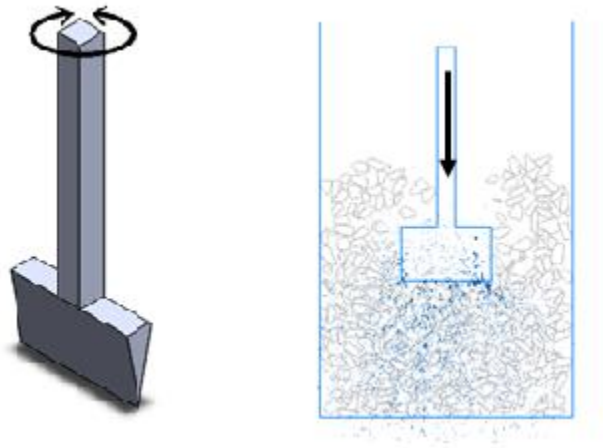

Figure 4.6 Illustration of the vibrating axis of the tamping tine (left) and penetration of ballast by the tine (right).

Lastly, material properties were assumed to be isotropic and material for both particles and the walls was set as basalt. The specification of material properties for basalt has been explained in the previous chapter, and following the same, the properties used for this simulation study are as listed in Table 4.1 below. The contact model chosen for modeling of both inter-particle and particle-wall contacts was Hertzian.

Table 4.1 Material properties used for the simulation study.

Property	**Value**
Mass Density (kg/m^3)	2750
Young's Modulus (GPa)	50
Poisson's Ratio	0.2
Friction Coefficient	0.6
Damping Coefficient	0.6

4.4.2 Results of the Simulation Study

The results obtained regarding the differences in the behavior of ballast by the virtue of the shape of the particles are discussed below.

Ballast Compaction

The ranges of compaction attained by all four gradations under consideration have been illustrated in Figure 4.7. The left end of the bars in the graphic represents the solid fraction of the naturally settled ballast whereas the right end denotes the solid fraction for the fully compacted ballast.

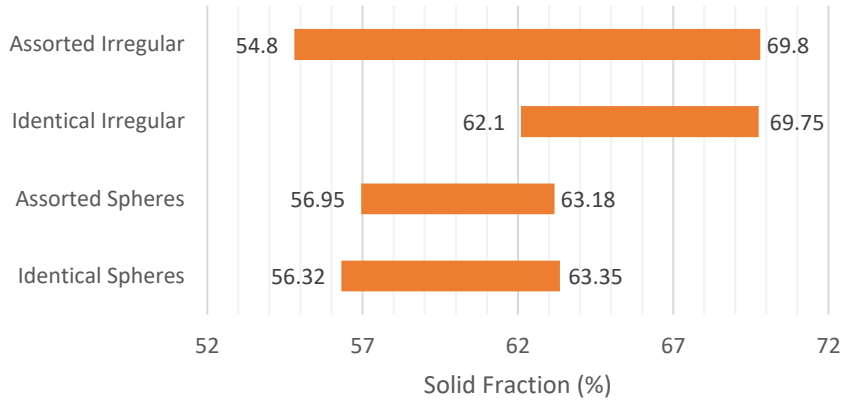

Figure 4.7 Percentage solid fraction achieved for different particle gradations. Naturally compacted state is marked on the left and the fully compacted state is marked on the right side of the bars.

The results show that disordered aggregates of spherical particles have a lower possible range of compaction compared to disordered aggregates of irregular particles of similar size. Absence of random projections and protuberances in spheres make them less effective at occupying interstitial void spaces among particles and achieving high vales of solid fraction. Consequently, modeling of ballast using spherical particles is likely to results in underestimation of actual ballast compaction below the sleeper, and therefore, track settlement rates. This difference in behavior is entirely due to the virtue of particles' shape and is unlikely to be affected by any possible discrepancies in contact physics. Additionally, it is theoretically not possible for a disordered arrangement of spheres to have solid fraction higher than 64% [57]. This implies that the

simulations were able to capture compaction of spheres with high accuracy and it is impossible to record ballast compaction beyond 64% using spherical particles of equal radii.

Coordination Number

Coordination number also shows similar trends as ballast compaction. As shown in Figure 4.8, spheres have lower coordination number than irregular particles throughout their state of compaction. This result can also be explained by the lack of random projections and protuberances in spheres, and their lower levels of compaction.

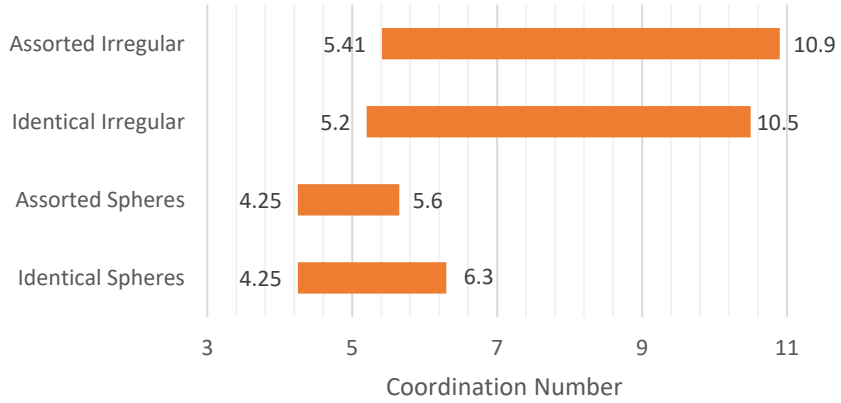

Figure 4.8 Coordination Number of particles for different ballast gradations. Naturally compacted state is marked on the left and fully compacted state is on the right side of the bars.

This implies that, when acted upon by a given load, spheres will experience higher load per contact compared to irregularly shaped particles, and there will be less diffusion of the load across the bulk of the ballast. Aggregates of irregular ballast particles, are therefore, more resilient to deformation.

Absolute Number of Contacts

The total combined number of inter-particle and particle-wall contacts in the container-ballast system is shown in Figure 4.9. Even though spheres and irregular particles have almost the same number of contacts in their naturally settled state, irregular particles have roughly twice as many contacts as spheres in their fully compacted state.

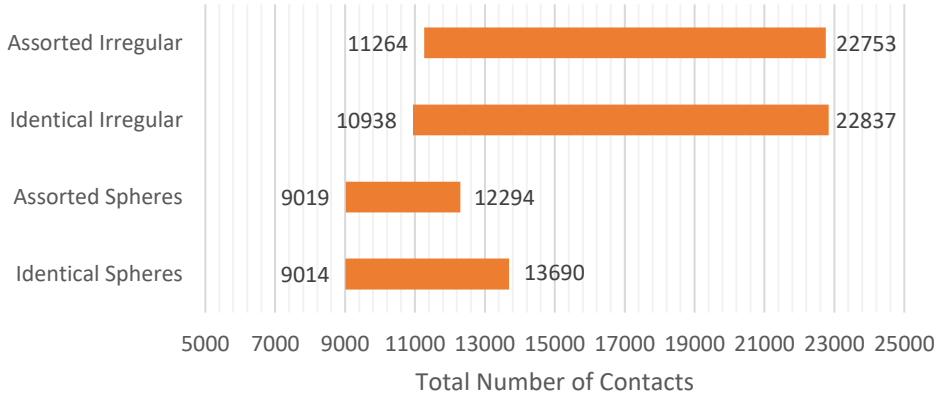

Figure 4.9 Total number of contacts in the assembly for different ballast gradations. Naturally compacted state is marked on the left and fully compacted state is on the right side of the bars.

This result is inclusive of particle-particle and particle-wall contacts. Number of particle-particle contacts corresponds to the coordination number, for particles with larger coordination number will have more number of particle-particle contacts for the same number of particles. It is also indicative of larger number of contacts between the particles and the walls of the container in the case of irregularly shaped particles. This implies that irregularly particles will have more number of contacts with a sleeper, for example, and will apply higher lateral frictional forces, thereby increasing lateral track stability. Measurements of lateral track stability based on simulation results of spherical particles will therefore, lead to underestimation of it.

Load Paths

The distribution of contact forces in naturally settled and fully compacted heaps of spheres and clumps has been compared in Figures 4.10 and 4.11 respectively. This distribution is similar for identical and assorted cases of both the modeled shapes. Magnitude and direction of contact force at every contact point is represented by a straight line with its thickness proportional to the magnitude and its orientation parallel to the direction of the force at that point. Figures 4.10a and 4.11a show the distribution of contact forces in naturally settled heaps of spheres and clumps respectively, whereas 4.10b and 4.11b show the distribution for fully compacted state of spheres and clumps respectively.

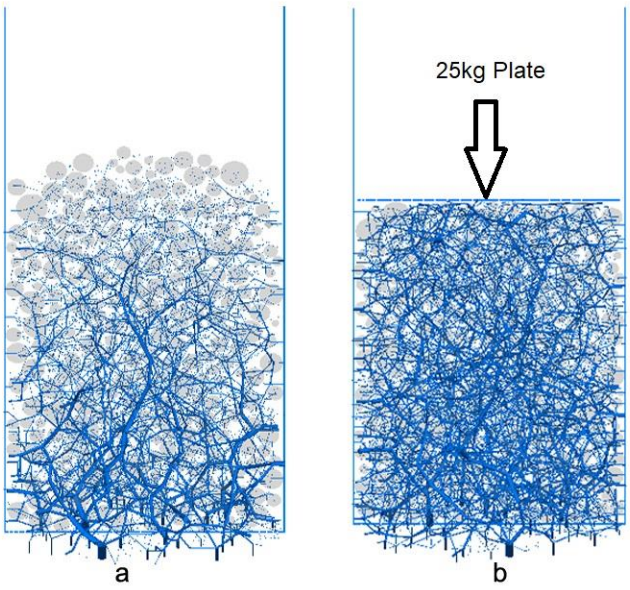

Figure 4.10 Distribution of contact forces for spherical particles within (a) the naturally settled ballast, and (b) fully compacted ballast.

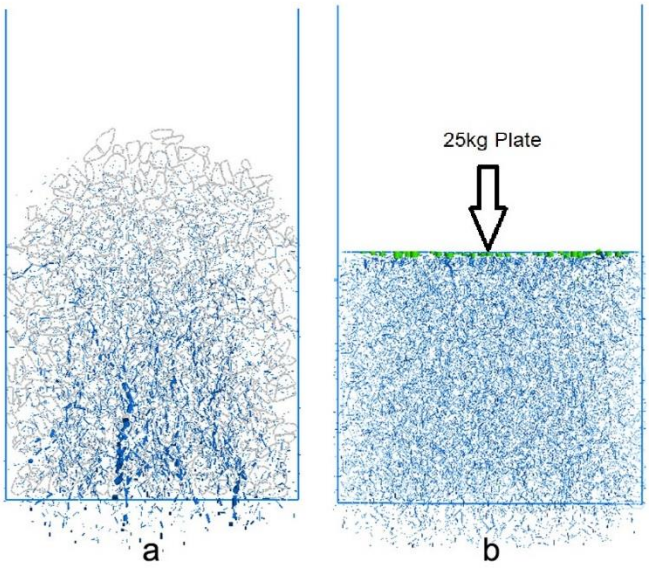

Figure 4.11 Distribution of contact forces for irregular particles (clumps) within (a) the naturally settled ballast, and (b) fully compacted ballast.

Since a pair of spheres can only have one mutual point of contact, with its normal aligned radially to both the spheres, contact forces form long bifurcated chains and provide branched but concentrated paths of load transmission. Distribution of external loads across the bulk of the heap,

therefore, is not uniform, and larger force is transmitted per contact. Alternatively, in the case of clumps, inter-particles contacts are arbitrary and their normal are haphazardly aligned. Therefore, any external force is diffused uniformly throughout the bulk of the heap.

Due to poor distribution of external loads and higher particle stresses under identical loading conditions, aggregates of spherical particle tend to yield at lower loads compared to aggregates of clumps. These results are in agreement with the conclusions drawn by Huang [14] and McDowell [28].

Vertical Contact Force on Tamping Tines

Figure 4.12 compares the net vertical force acting on tamping tine during insertion into the ballast. A moving average filter has been applied on the raw data to remove the high frequency fluctuations arising from collisions of the tine with individual particles. Trends show that spheres have much lower resistance to penetration by tines compared to clumps. Additionally, the resistance to penetration increases linearly with the depth of insertion in case of spheres whereas the growth is significantly more arbitrary for clumps. Therefore, estimates of power requirements of the tamping equipment and design of tine shape are likely to be negatively affected if spheres are used.

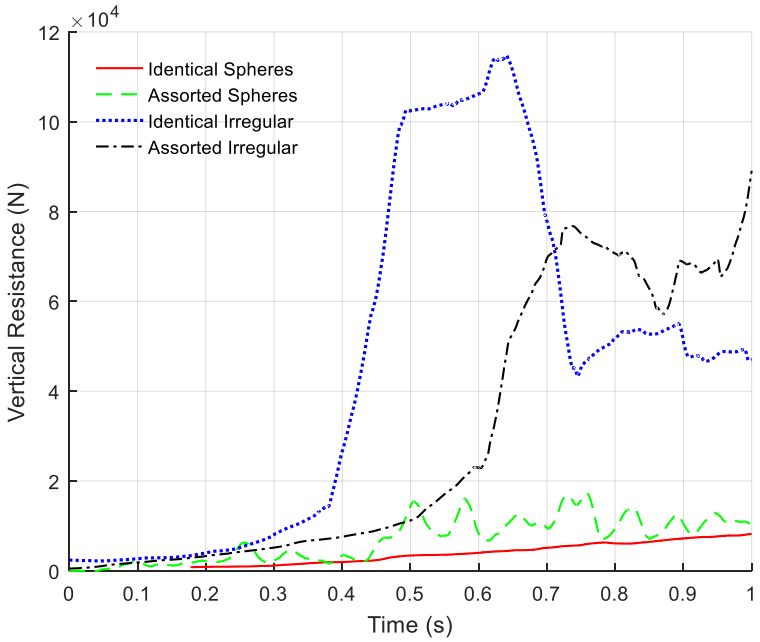

Figure 4.12 Comparison of resistance offered by the ballast to the insertion of a vibrating tamping tine for different particle gradations.

Simulation Time

The total time taken for the simulation to reach solution in each case was recorded for the comparison of performance. The recorded time data has been rounded off to the nearest hour and encapsulated in Table 4.2. All simulations were performed on same hardware and simulation code was identical in all cases except for the particle gradations. Since the simulation time is dependent on the capability of the hardware, this data can only be used for relative comparison of computational resource intensity of each of the studied gradations.

Table 4.2 Total time taken by one simulation run (rounded to nearest hour) for reaching complete solution in different cases. All simulations were performed on the same hardware.

Ballast Particle Shapes	**Simulation Time (hours)**		
	Initial Settlement of Ballast into the Container	Complete Compaction of Ballast after Settlement	Insertion of Tamping Tool into the Ballast
Identical Spheres	6	33	2
Assorted Spheres	8	47	3
Identical Irregular	52	132	7
Assorted Irregular	81	179	9

The table shows expected trends. Simulation time increases as the complexity of particle gradations increases, resulting in increasing number of contacts needing resolution per time-step and sophistication of kinematics of complicated particle shapes.

4.4.3 Conclusions

The goal of this study was to analyze the anomalies presented by use of spherical shape to model irregularly shaped railway ballast particles. Results of simulations performed indicate that there are fundamental differences between behavior of spherical particles and irregularly shaped particles in granular assemblies entirely due to virtue of their shape. Although models using

spherical particles are much more computationally efficient, agglomerates of spherical particles are physically incapable of capturing the entire range of granular compaction possible in case of the irregularly shaped particles. The number of contacts which each spherical particle has with its adjacent particles or bodies is also lower compared to the irregularly shaped particles. Further, the particle shape has a bearing on the predominant mechanism of load transmission within the granular assembly, which dictates the nature of response the assembly will have to external loads. These differences cannot be mitigated by employing artificial contact physics between particles and might results in discrepancies in simulation results if spherical shape is used to model railway ballast. For example, as shown in this study, granular assemblies made of spherical particles have lower resistance to penetration by tamping tools compared to those of irregularly shaped particles. Additionally, absolute gain or loss in ballast compaction after tamping will not be earnestly captured by spheres, resulting in errors in track stability estimates. Therefore, approximating irregularly shaped particles using spherical shape for studying holistic behavior of railway ballast is not recommended.

5. Simulation Model of Tamping

This chapter covers the construction of a simulation model of tamping using DEM and the tools provided by PFC^{3D}. Configuration of a discrete element model in PFC^{3D} requires systematic specification of various model components regarding the simulation environment, properties and behavior of physical bodies, and solution criteria. This configuration of the simulation and the model is carried out using a script of code. PFC^{3D} uses a command line interface and all scripting is done using the FISH language. A script constitutes several sections of code corresponding to definition of the following-

1. Simulation domain,
2. Particle and wall geometry,
3. Particle and wall contact properties,
4. Simulation physics and wall motion,
5. Output variables, and,
6. Solution criteria.

PFC^{3D} offers some flexibility in order of the definition of these components within the script. Additionally, a few components are optional or have preset default values, and therefore, do not require explicit definition. The beginning and the end of a script also contain some ancillary commands for loading, closing, and saving of data files.

5.1 The Half-Track Model

Features of symmetry can be utilized to reduce the size of the simulation model and the amount of calculation required to obtain solution. Since tamping process is performed symmetrically about the common longitudinal axis of the pair of rails, therefore, only one half (left or right) of the track structure needs to be modeled. Additionally, all sleepers being tamped are subjected to identical input, and therefore only one sleeper will be simulated. Both rails are excluded for simplicity and

the only physical bodies modeled apart from the ballast particles are sleeper and tines. Traffic loads are directly applied to the sleeper. Figure 5.1 highlights the components of the rail track structure being modeled.

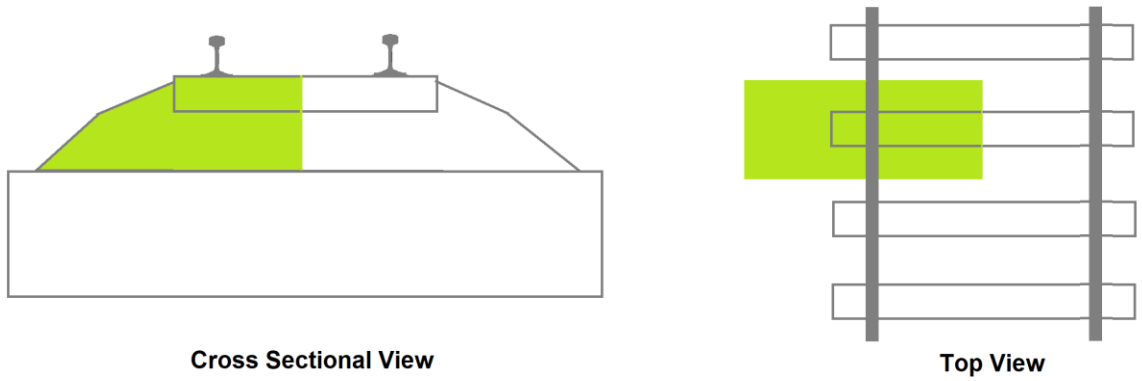

Figure 5.1 Modeled section of a complete rail track structure, highlighted in green, is shown in cross-sectional view (left) and top view (right). It includes half of a sleeper and volume of ballast surrounding the sleeper as shown.

Apart from the symmetry, other assumptions and approximations involved in the Half-Track model are-

1. Any influence on ballast due to sleepers adjacent to the sleeper being tamped is ignored for simplicity.
2. Breakage and fracture of ballast particles due to squeezing forces from tamping is ignored.
3. Since sleepers on a track are tamped in a sequential manner, ballast condition at the front of the sleeper being tamped is different than at its rear. Although for simplicity in the model, the ballast is modeled to be identical at the front and the rear of the sleeper, since pressure based squeezing action of the tamping tines is designed to compensate for the difference nonetheless.
4. Entire motion of the tamping tines except the squeezing action is assumed to be at constant velocity.

5.1.1 Information Flow in the Model

PFC^{3D} allows the user to incorporate functional modularity into the simulation script by discretizing the code into separate blocks of code. Each block of code can be saved as a separate data file and can be worked on independent of other data files within the same simulation project. This capability offers multiple practical advantages, including the following:

- The solution can be saved at different stages of progress. It is critical since the total simulation time can reach several weeks and any undesirable event like a power interruption or processor overheating can potentially lead to loss of all data.
- Troubleshooting and bug fixing within the script is streamlined because separate blocks of code can be run and tested independently.
- User does not need to write the entire code before running the simulation. Since solving one block of code can potentially take a long time, data file corresponding to the next stage of simulation can be written and debugged while the previous one is solving.
- Certain blocks of code might require repetitive solution within one simulation study. For example, testing various tamping parameters for a comparative study requires repetitive generation of initial condition of ballast before tamping. Such cases can be handled in a computational and time effective manner by saving the initial condition of ballast in a separate data file and loading it before the code corresponding to tamping is run.

These features of PFC^{3D} have been utilized to create a structured and robust information flow within the simulation model. The schematic representing the information flow is shown in Figure 5.2.

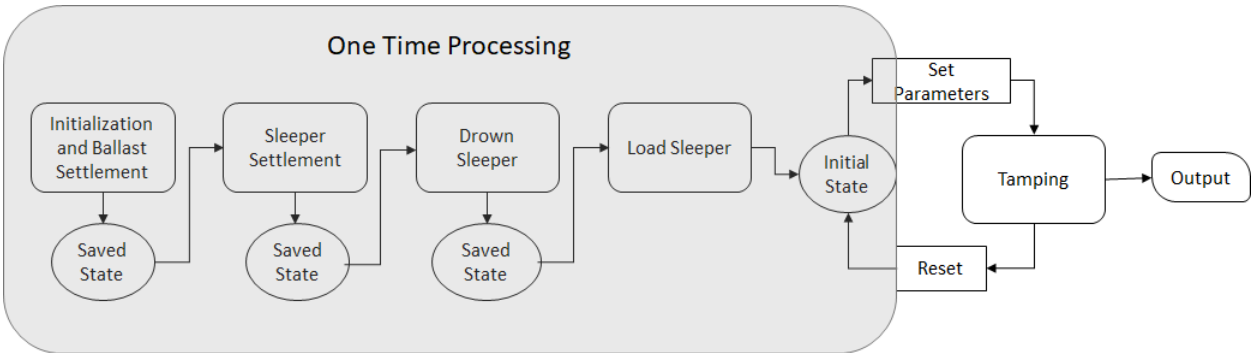

Figure 5.2 Information flow and data structure of the simulation model code script.

Functionality of various data files in the simulation model is as described next.

1. Ballast Generation and Settlement

This data file creates a new simulation project and deals with initialization of the simulation environment, definition of container for ballast, definition of physics including contact models and material properties for all bodies, definition of ballast gradation and consequential generation of particles, and finally, the settlement of the generated ballast particles under gravity until a specified target criterion, such as compaction, is met. After this file is completely run, the settled ballast gets saved as a standalone model state.

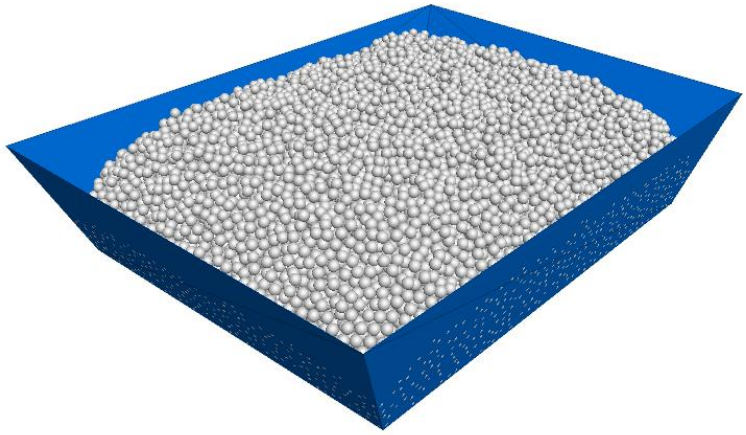

Figure 5.3 Generated (spherical) ballast particles settled after the execution of first data file.

2. Sleeper Settlement

The settled ballast state, saved by the previous data file, is loaded and a half-sleeper is generated in the simulation environment. The sleeper is assigned a mass and is made to settle on the top of settled ballast particles under the influence of gravity until the net unbalanced force on the sleeper reaches below a specified threshold. The settled sleeper is then saved as a new model state.

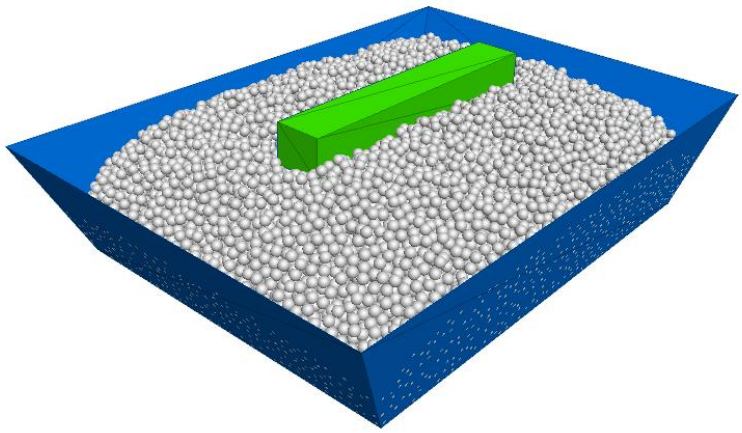

Figure 5.4 Generation and settlement of the half-sleeper on the already settled ballast in the second data file.

3. Drown Sleeper

The settled sleeper state is loaded, and additional ballast particles are generated around the periphery of the sleeper such that all its vertical faces are covered by ballast and only its top horizontal face is left uncovered. Gradation so this ballast is identical to the previously specified gradation. This generation of ballast around sleeper corresponds to actual track laying process where additional ballast is dumped after a track has been laid. This generated ballast is then allowed to settle until velocity of all individual particles is close to zero. Latest model state is finally saved in the end.

4. Load Sleeper

This data file replicates traffic loading cycles on the settled sleeper to obtain realistic compaction state of ballast below the sleeper. If compaction of ballast below the sleeper is already known, then it can instead be modeled in the first data file and this file can be omitted from the model. The output of this file is saved as the final state of the model before tamping and is loaded while simulating different tamping parameters. Therefore, data files 1 to 4 are only required to be solved once during the starting of the study.

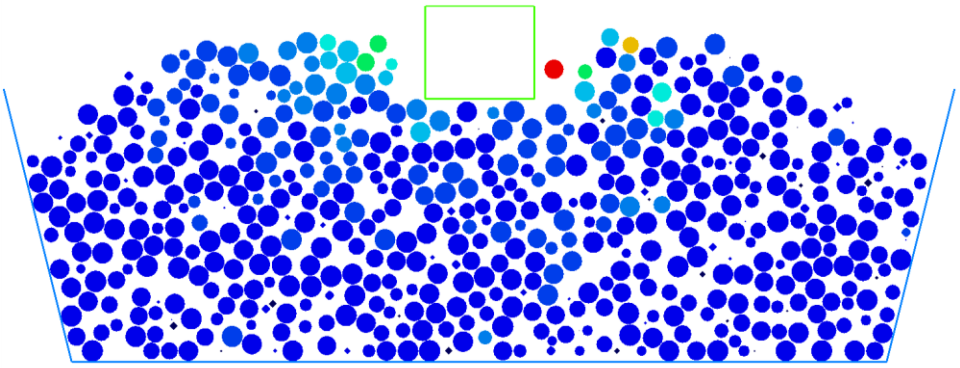

Figure 5.5 Cross-sectional view of sleeper position after its final settlement due to loading at end of fourth data file. This is also the initial ballast state before tamping.

5. Tamping

Tamping is the last data file. It loads the last saved ballast state, import tine geometry, lifts the sleeper up, and performs tamping operation on it according to the values of the parameters defined in the script within the file. All final output variables are recorded in the results of this file and saved as the final result for the associated tamping parameters. For conducting the study for comparing different parameters, only this file needs to be run repeatedly after changing the parameter values within the script.

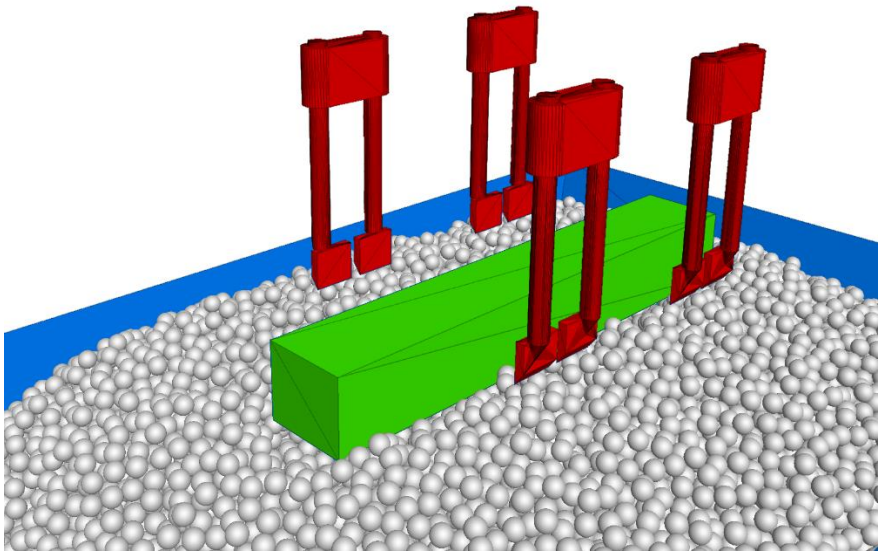

Figure 5.6 Generation of tamping tines and execution of one tamping cycle in the last data file.

5.2 Boundary Conditions

Boundary conditions are specified for the ballast in the simulation. Boundary conditions can be utilized to mimic effects of a large number of particles, reducing the overall number of particles in the simulation and consequently, the simulation time. Two types of boundary conditions have been used in the tamping model-

1. Periodic Boundary

Whenever a boundary is specified as periodic in PFC^{3D}, the particles exiting that boundary are made to re-enter from the opposite side of the model boundary. In a densely populated granular system like railway ballast, periodic boundary can be used to replicate effects of 'infinite' ballast, i.e., the boundary acts like a flexible wall of ballast particles and the granular system has no effective edges.

2. Open Boundary

In open boundary, the granular system has an edge beyond which no other particles exist. Particles at the open boundary are in contact with other particles from only one side, whereas the other edge is open to the environment.

Figure 5.7 shows the edges of the model that are modeled as periodic and open boundaries. The faces of the track cross section whereas other ballast particles would exist in real world are modeled as periodic boundaries, whereas the lateral sides of the track structure and the top face are modeled as open boundary.

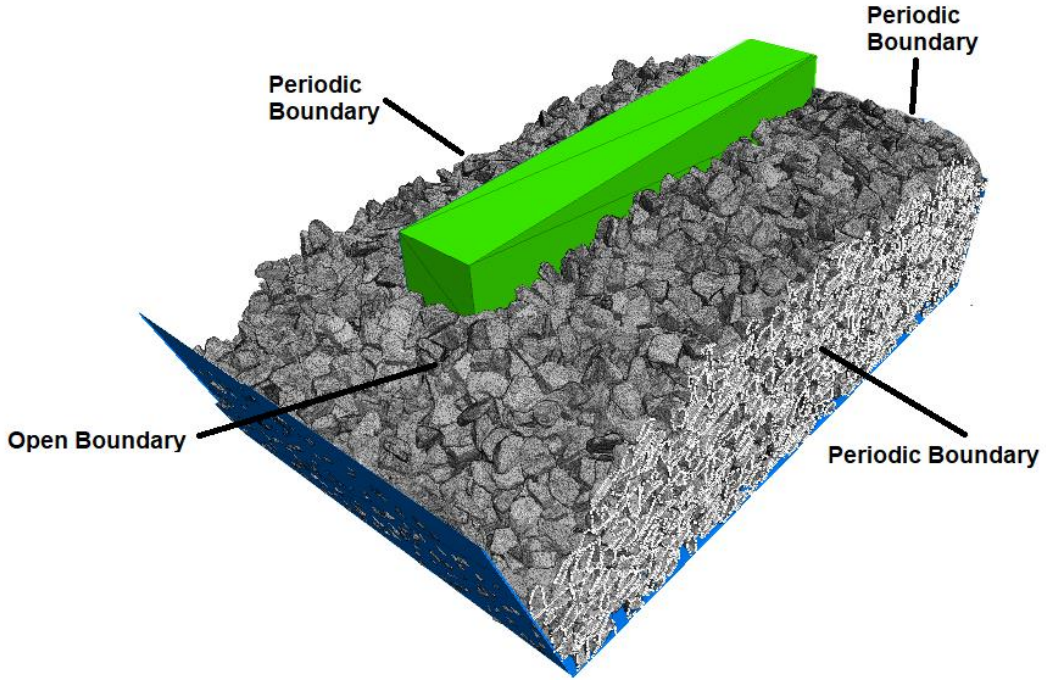

Figure 5.7 Location and types of boundary conditions for the ballast. Reduction in number of modeled particles by the introduction of periodic boundary conditions is emphasized.

5.3 Initial Condition

Initial condition refers to the state of the model before the ballast is tamped. It affects the track stability achieved after tamping and is dependent on the state of ballast only. The initial condition of ballast, in turn, is influenced by it gradation, state of contamination or fouling, and its compaction. Factors other than compaction are held constant throughout a simulation, and are therefore, classified as input parameters instead. Initial compaction of the ballast can range between 55% and 66% [17], and can be replicated within the model during generation of ballast particles. PFC^{3D} directly supports generation of particles at a desired level of compaction or with a certain packing arrangement.

Alternatively, if initial compaction is not known accurately, naturally settled ballast can also be compacted by applying traffic loading cycles on the sleeper. This method of compacting ballast is more realistic, but more computationally intensive. A typical loading cycle on a sleeper during

traversing of train can be modeled as a combination of two sine waves as shown in Figure 5.8 [58, 59].

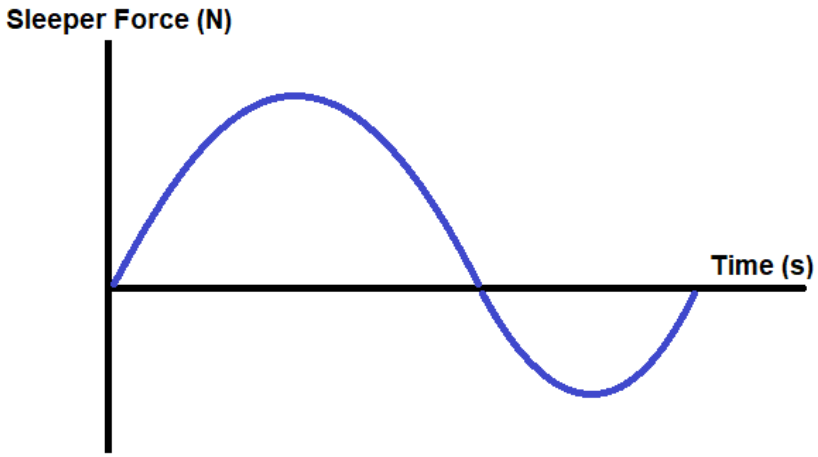

Figure 5.8 Representation of forcing function for a sleeper during passing of a train axle.

Positive peak in the cycle denotes vertically downward load, whereas the negative peak denotes the upward force on the sleeper during loading of neighboring sleepers. The peak amplitudes of the pulses are primarily dependent on the axle load of traffic. Amplitude of the negative pulse is also dependent on spacing between consecutive sleepers. Additionally, the frequency of pulses is characterized by traffic speed. Practically, track settlement occurs over millions of such loading cycles, but it is impractical to simulate such a large number cycles virtually due to large computational requirements. Therefore, more feasible alternative loading cycles could be further investigated by scaling magnitude or frequency of actual loading cycles so that similar compaction could be obtained for a lower number of cycles.

5.4 Input Parameters and Variables

Input variables for the tamping model can be classified in three categories-

- Parameters for configuration of model physics,
- parameters defining ballast gradation and behavior, and
- process variables of tamping

Parameters related to model physics and ballast, even though act as input to the model, are held constant throughout the project once set and are not the focus of the study. These parameters have already been discussed in detail in Chapters 3 and 4 respectively because of their significant influence on the quality of results obtained from the model. Input parameters and variables corresponding to simulation of tamping in the model including the following:

1. Sleeper Lift

It is the vertical height by which the sleeper is lifted from its originally settled position before start of the tamping cycle.

2. Shape of Tamping Tines

Overall geometrical shape and features of the tines form the first input to the model. The geometrical designed can be prepared in a CAD package and imported into PFC^{3D} in *stl* file format. Figure 5.9 shows a simplified pair of tines used in the tamping model.

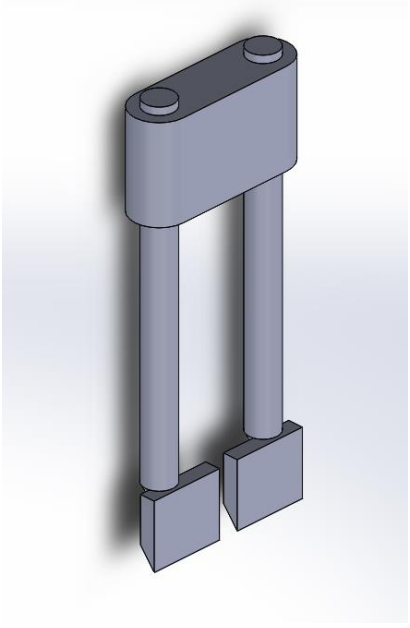

Figure 5.9 CAD representation of the pair of modeled tamping tines.

3. Motion of Tamping Tines

The motion of tines during one cycle of tamping a sleeper is subdivided into 4 steps- insertion, squeezing, release, and withdrawal. These cyclic steps of motion of a set of tines have been

depicted in Figure 5.10. The squeezing and release of ballast below the sleeper has been modeled as parallel traversing of opposite pair of tines towards and away from each other. It can alternatively be modeled as clockwise and anti-clockwise rotation of the opposite pairs about a remote axis of rotation.

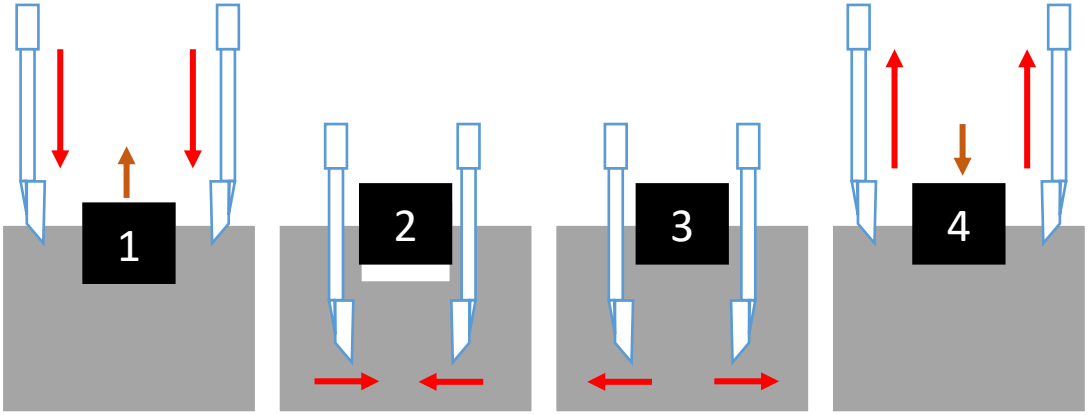

Figure 5.10 Steps of motion of tines for one tamping cycle.

4. Characteristic Trajectory of Tine Vibration

There are usually 8 pairs of tines acting per sleeper during tamping, 4 pairs around either rail. As specified in Chapter 2, each pair is vibrating continuously along its vertical axis throughout operation. The motion of a pair during vibration can have several different possibilities and the nature of this trajectory greatly influences the results achieved by the equipment. Different manufacturers use different types of characteristic trajectories of tine vibration, and these trajectories, along with a few other possibilities have been depicted in Figure 5.11. The mathematical expression describing this vibration as a function of time is input by the user.

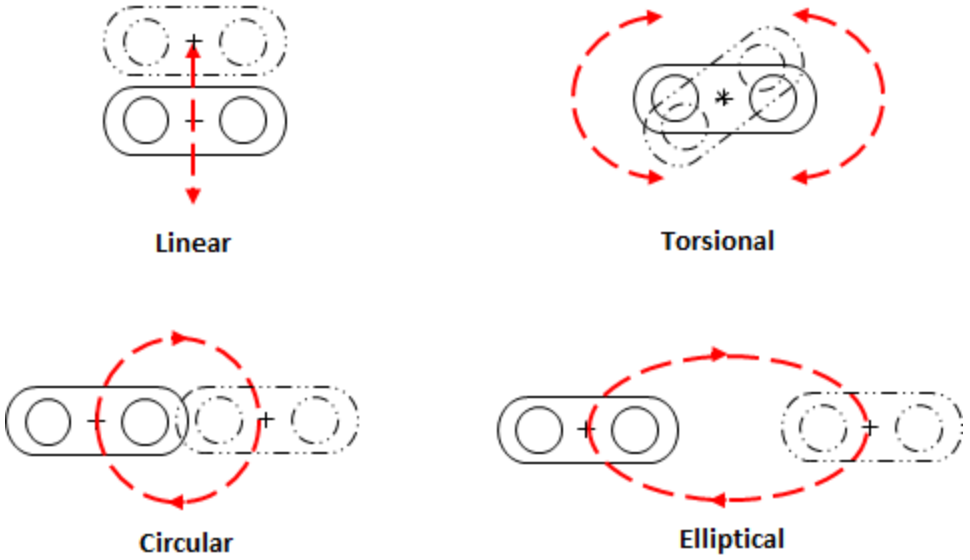

Figure 5.11 Various characteristic vibratory motions of tamping tines.

5. Frequency of Vibration

The frequency of vibration of tines is a required input for the tamping model. This frequency is associated with liquefaction of ballast while tamping and is a critical parameter for controlling the ballast compaction below the sleepers.

6. Amplitude of Vibration

The amplitude of the vibration of the tines needs to be specified as: a length measurement for linearly vibrating tines, an angle measurement for torsional vibration, and a mathematical function for vibrations with a closed loop trajectory.

7. Insertion Velocity

Tines are assumed to be inserted into the ballast with a constant downward velocity. This velocity is programmed by the user and tines travel downward at this rate until the desired depth is reached.

8. Depth of Insertion

The vertical depth below the sleeper until which tines are inserted with a constant velocity is also set as an input variable for the user.

9. Squeezing Force

Once the tines have penetrated the ballast to the set depth below the sleeper, opposing pairs of tines move horizontally towards each other in a force controlled manner. This force has to be

proportional to the practically used values of squeezing pressure since PFC3D does not allow specification of pressure values directly.

10. Squeezing Limit

Squeezing limit adds a secondary layer of control to the squeezing motion of tines. In case that squeezing pressure is set to a large enough value that squeezing motion of tines cannot be countered by the ballast pressure, squeezing limit defines the minimum distance between the opposing pairs of tines at which the squeezing action will be halted before the pairs collide with each other and crush the ballast particles trapped between them.

11. Squeeze Hold Time

This occurs over a short duration for which the motion of the tines is paused between step 2 and 3 as shown in Figure 5.10. This pause allows the compacted ballast particles to come to rest and maintain the arrangement created by the squeezing motion of the tines.

12. Release Velocity

After reaching the set squeezing pressure, the tines are retracted horizontally (Step 3) with a constant velocity set by the user.

13. Withdrawal Velocity

It is the input value which specifies the constant velocity at which the tines are withdrawn from the ballast vertically. It is the last step of one tamping cycle.

5.5 Output Variables and Graphics

PFC^{3D} records all output variables against the history of simulation time-steps. The following variables are saved as output of the simulation-

1. Simulation Time

It records cumulative time elapsed as a history of number of individual time-steps. Therefore, every element of this time vector is a sum of all previous time-steps. Since, all other variables are recorded against number of time-steps as well, this variable allows synchronizing of output data with the events of the simulation in post processing.

2. Ballast Compaction

Ballast compaction is expressed as solid fraction, i.e., the percentage of total volume occupied by solid mass of ballast particles. PFC^{3D} calculates solid fraction by means of 'measurement spheres', which have been discussed in detail in the next section.

3. Ballast Coordination Number

Ballast coordination number is also calculated as a measure of stability of a particular arrangement of ballast particles. Measurement spheres, as described in the next section, are also used for calculation of this output variable.

4. Ballast Particle Stress

Individual stress components and net stress value of ballast particles is recorded by the use of measurement spheres as well. These stress values are indicative of crushing forces exerted by the tamping tines on the ballast particles due to a particular squeezing pressure value.

5. Contact Forces on Tines

Contact forces acting on tamping tines during their motion inside the ballast are recorded for studying the relative power requirements of tamping based on tine design and ballast gradations. Individual vector components and the net resultant force is recorded for all pairs of tines at every time-step.

6. Graphical Load Distribution

The distribution of external loading and excitation from the sleeper and the tines across the volume of the ballast is plotted at every time-step, but no numerical data is recorded. This distribution is shown by representing contact force components at all contact points within the model with vectors scaled in thickness proportional to their magnitude and aligned parallel to the orientation of the force. Such load distribution graphics have been depicted in Figures 4.10 and 4.11 previously. These graphical plots can be saved as a series of sequential model states at every time-step in form of a video clip.

5.5.1 Measurement Spheres

PFC^{3D} only allows recording of mesoscopic properties of particles through use of measurement spheres. A measurement sphere is a user defined spherical volume in the simulation environment

which monitors selected properties for all particles lying within or intersecting with the sphere. It has no influence on physics of the model at all.

The measurement sphere is configured by the user by specifying its center coordinates and the radius length such that it encloses the volume of interest in the simulation environment. During the simulation, the ballast properties are calculated for a given measurement sphere as follows

Solid Fraction

Solid fraction, s, is defined as the ratio of cumulative volume of all particles within the sphere, V^{sol}, to volume of the sphere, V^{sph}-

$$s = \frac{V^{sol}}{V^{sph}} \tag{5.1}$$

And,

$$V^{sol} = \sum_{N_b} V^b \sum_{\bar{N}_b} \bar{V}^b - \sum_{N_c} V^c \tag{5.2}$$

Where,

N^b is the number of bodies completely within the sphere,

V^b is the volume of the body b,

$\bar{N}^b$ is the number of bodies intersecting the sphere,

$\bar{V}^b$ is the partial volume of the body b within the sphere,

N^c is the number of inter-particle contacts within the sphere, and

V^c is the overlap volume of the pair of bodies at contact c

The partial volume of an intersecting clump lying inside the measurement sphere, $\bar{V}^b$, is calculated using a sophisticated voxelization algorithm built inside PFC^{3D} and has not been discussed here.

Coordination Number

Coordination number, C_n, is the average number of active contacts a particle has with its immediate neighboring bodies-

$$C_n = \frac{\sum_{N_b} n_c^b}{N_b} \tag{5.3}$$

Where,

N^b is the number of bodies with their centroids within the sphere, and

n_c^b is the number of active contacts of body b

Stress

Stress is a property of the continuum and the stress measurement of discrete particles is represented by averaging the individual calculations for all particles present within the measurement sphere-

$$\bar{\sigma} = -\frac{1}{V^{sph}} \sum_{N_c} F^c \otimes L^c \tag{5.4}$$

Where,

$\bar{\sigma}$ is the average stress in the measurement sphere,

V^{sph} is the volume of the measurement sphere,

F^c is the contact force vector,

L^c is the vector joining the centroids of the two bodies in contact, and

$\otimes$ is the outer product

Compressive stresses are negative by convention.

Since calculation of these variables is limited to only the extent of the measurement sphere, and not the entire bulk of the ballast in the simulation model, multiple measurement spheres are configured to record output at all different points of interest below the sleeper as shown in Figure 5.12.

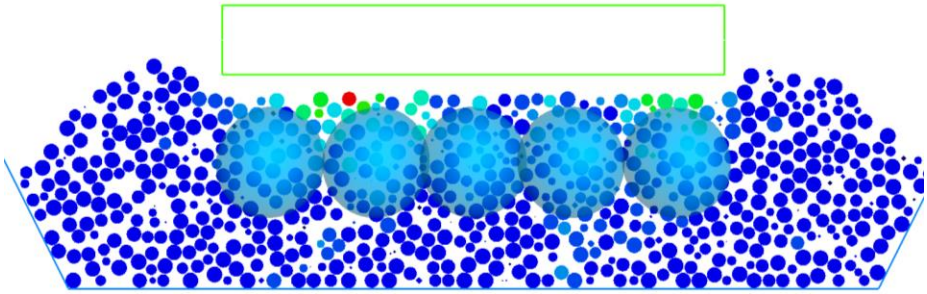

Figure 5.12 Configuration of measuring spheres below the sleeper for recording output data during simulations.

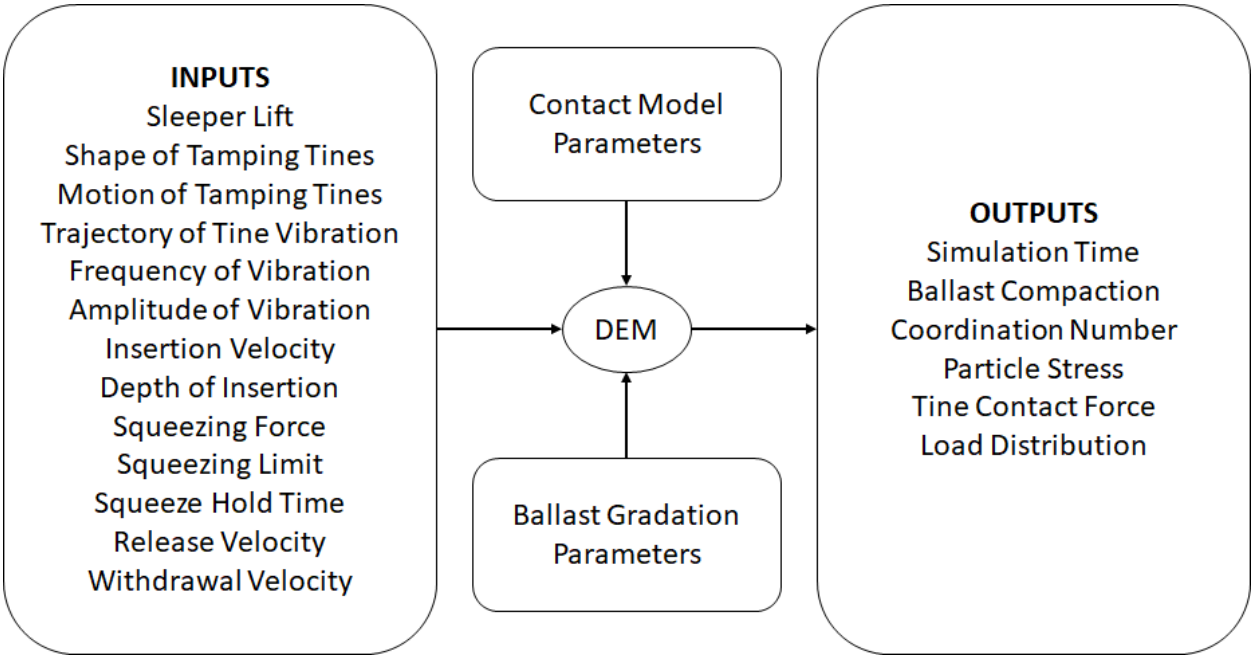

Figure 5.13 Schematic of the information flow structure of the tamping simulation model.

6. Summary and Conclusions

6.1 Summary of Results

A comprehensive literature review of track stability, tamping, and DEM was presented in Chapter 2. Current knowledge establishes that track stability, both in vertical and lateral directions, is dependent on mechanical properties of the ballast and tamping is a proven maintenance technique for restoring defects in track geometry. The ability of tamping operation in achieving sustainable track stability can be analyzed by studying the behavior of ballast particles undergoing tamping and scrutinizing the ballast parameters which affect track stability such as, ballast compaction, coordination number, and stress. These ballast properties are impractical to measure physically but can be credibly examined using the Discrete Element Modeling (DEM) techniques.

Chapter 3 dealt with modeling of contact physics and configuration of concerned parameters. Mathematical formulation of four most commonly used contact models was presented and compared, and it was established that the Hertz model is best suited for modeling contact between ballast particles. Hertz contact model is specifically suited for modeling low velocity collisions between highly stiff bodies, and accurately captures the contact force verses particle overlap behavior found experimentally. Additionally, model parameters for the Hertz model can be directly calculated from material properties of the bodies and therefore, are much easier to calibrate compared to parameters of the Linear contact model which have no physical significance.

Different methods of capturing particle shape information were presented in Chapter 4. A simulation study was also undertaken to compare the performance of different ways of modeling particle shapes. A direct comparison of ballast properties relevant to tamping between spheres and clumps revealed that particle shape has significant influence the quality of results obtained from DEM simulations. Granular aggregates made of spherical particles compact less tightly compared to the aggregates of clumps, and their coordination number is lower as well. Spherical particles

showed a maximum compaction limit of 63.35% and highest coordination number of 6.3, meanwhile these limits for the clumps were 69.8% and 10.9 respectively. Significant differences also exist in the mechanism of load transfer within these two types of granular aggregates. Aggregates of spherical particles transfer loads via concentrated and branched chains of inter-particle contacts whereas clumps diffuse the external load almost uniformly throughout the bulk of the aggregate. This implies that using spherical particles for simulating tamping operation might not only skew estimates of resulting track stability, but will also lead to unrealistic mechanical behavior under traffic loading. Another major point of difference was the magnitude of resistance provided by the ballast to penetration by tamping tines. Spherical particles were found to apply much lower contact forces on tamping tines compared to clumps, resulting in underestimation of power required for executing tamping cycle. Finally, although clumps evidently lead to more accurate results in terms of overall mechanical behavior, they were found to have significantly higher computational cost compared to spheres, leading to solution times being longer by several orders of magnitude. Therefore, a deliberate compromise is to be made between accuracy and computational economy while designing the simulations regarding holistic goals of the study.

In the previous chapter, development of a tamping simulation model was presented. Exploiting the symmetry in tamping, a half-track model has been prepared. Simplifying assumptions involved in the model were encapsulated and the importance of data files in inducing modularity into the simulation code was discussed. Based on the features available in PFC3D, a user-friendly code script was developed for easy troubleshooting, high flexibility in execution, and high simulation turnover rate. Two types of boundary conditions, periodic and open, were introduced and their application at various regions in the simulation environment was explained. Boundaries of the ballast that have contact with other ballast particles were modeled as periodic, and all other boundaries were modeled as open. Different methods of replicating initial compaction of the ballast before tamping were also discussed. Lastly, 13 input variables and six output variables of the model were identified and methods of their determination were specified.

6.2 Extended Utility of the Ballast Model

Since all ballast-related track behavior can be captured using DEM techniques, the model developed in this research can be extended for undertaking general studies related to railway ties (sleepers) and ballasts, such as:

1. Different track maintenance methods like Dynamic Track Stabilization (DTS), Stone blowing, etc. can also be simulated and compared with each other [45].
2. Improvements in track stability can be analyzed by comparing performance of different sleeper designs and materials [46].
3. Geometrical features of tamping tines can be further developed to improve their efficacy by reducing particle breakage, maximizing particle mobilization, increasing service life, and lowering power requirements.
4. Different ballast gradations can be compared to study their effect on track stability, including effects of fouling and contamination of ballast. Differences in response of fouled or contaminated ballast to tamping can also be explored.
5. Influence of factors like traffic speed, axle loads, and loading frequency on track settlement rates can be investigated using DEM as well.
6. Development of engineered ballast gradations and instrumented ballast particles for data acquisition has been an area of recent interest. DEM techniques are invaluable in research and design of such advanced ballast systems.

6.3 Future Studies

Model parameters pertaining to physics and contact behavior of the bodies require experiment based calibration for ensuring validity of the simulation results. Contact parameters like frictional behavior, contact stiffness, contact damping, and contact force laws are calibrated using a series of standardized physical tests and experiments discussed in Chapter 3. This ensures accuracy of mesoscopic ballast properties and gross ballast behavior in the model.

Second category of parameter that requires calibration affects the accuracy of the mechanical behavior of the bodies and determines the computational costs of the model. This category includes

geometrical parameters of the model like particle shape, and particle shape detail and their calibration was discussed in Chapter 4.

After due calibration of the aforementioned model parameters as discussed, a parametric study of the tamping process could be performed, and recommendations could be made to improve current industry practices.

References

1. Lichtberger, B., *Track Compendium* 2011, Hamburg: Eurail Press.
2. Kerchof, B., *Research and Tests at Norfolk Southern*. November 17, 2016: Virginia Tech-Railway Technologies Laboratory Annual Review- Personal Communication.
3. Wachsmuth, J., *Technology Engineer at Norfolk Southern*. March 28, 2017, E-mail Correspodence
4. Audley, M. and J. Andrews, *The effects of tamping on railway track geometry degradation.* Proceedings of the Institution of Mechanical Engineers, Part F: Journal of rail and rapid transit, 2013. **227**(4): p. 376-391.
5. Koc, W., et al., *Tests on lateral resistance in railway tracks during the operation of a tamping machine*. Proceedings of the Institution of Mechanical Engineers, Part F: Journal of Rail and Rapid Transit, 2011. **225**(3): p. 325-340.
6. Soleimanmeigouni, I., et al., *Evaluation of the effect of tamping on the track geometry condition: A case study*. Proceedings of the Institution of Mechanical Engineers, Part F: Journal of Rail and Rapid Transit, 2016: p. 0954409716671548.
7. Cundall, P.A. and O.D. Strack, *A discrete numerical model for granular assemblies.* geotechnique, 1979. **29**(1): p. 47-65.
8. Esveld, C., et al., *Historic data on track geometry in relation to maintenance.* Rail Engineering International, Edition, 1988(2): p. p16.
9. Suiker, A.S.J., *The mechanical behaviour of ballasted railway tracks*. 2002.
10. Telegraph, T. http://www.telegraph.co.uk/news/weather/11707973/Travel-chaos-forecast-as-35C-heatwave-could-buckle-train-tracks-and-melt-roads.html, *Newspaper Article*. 2015.
11. Plasser&Theurer, https://commons.wikimedia.org/wiki/File:Plasser_%26_Theurer_ballast_tamper,_Chester_Railway_Station_-_DSC05883.JPG. 2010.
12. Rail-Geelong, https://www.railgeelong.com/gallery/events/north-shore-crossing/D352_5234.jpg.html. 2007.
13. Plasser&Theurer, https://www.plassertheurer.com/en/machines-systems/tamping.html.
14. Tutumluer, E., et al. *Aggregate shape effects on ballast tamping and railroad track lateral stability*. in *AREMA Annual Conference, Loisville, KY, Sept*. 2006.
15. Itasca Consulting Group, I., *PFC — Particle Flow Code, Ver. 5.0. Minneapolis: Itasca.* 2014.
16. Cundall, P.A. and R.D. Hart, *Numerical modelling of discontinua.* Engineering computations, 1992. **9**(2): p. 101-113.
17. Tutumluer, E., et al. *Field validated discrete element model for railroad ballast*. in *Proc., Annual Conference of the American Railway Engineering and Maintenance-of-Way Association*. 2011.

18. Tutumluer, E., et al. *Discrete element modeling of railroad ballast settlement*. in *AREMA conference*. 2007.
19. Lu, M., *Discrete Element Modelling of Railway Ballast*. 2008, The University of Nottingham. p. 245.
20. González, J.I., E.O.I. de Navarra, and F.S. González, *NUMERICAL MODELLING OF RAILWAY BALLAST USING THE DISCRETE ELEMENT METHOD*. 2015.
21. Cholet, C., et al. *Study of the mechanical behaviour of the ballast using discrete approach*. in *Tagungsband des World Congress on Railway Research, Köln*. 2001.
22. Stahl, M. and H. Konietzky, *Discrete element simulation of ballast and gravel under special consideration of grain-shape, grain-size and relative density.* Granular Matter, 2011. **13**(4): p. 417-428.
23. Hossain, Z., et al., *DEM analysis of angular ballast breakage under cyclic loading.* Geomechanics and Geoengineering: An International Journal, 2007. **2**(3): p. 175-181.
24. Saussine, G., et al., *Modelling ballast behaviour under dynamic loading. Part 1: A 2D polygonal discrete element method approach.* Computer methods in applied mechanics and engineering, 2006. **195**(19): p. 2841-2859.
25. Indraratna, B., et al., *Behavior of fresh and fouled railway ballast subjected to direct shear testing: Discrete element simulation.* International Journal of Geomechanics, 2012. **14**(1): p. 34-44.
26. Lu, M. and G. McDowell, *Discrete element modelling of railway ballast under monotonic and cyclic triaxial loading.* Géotechnique, 2010. **60**(6): p. 459-467.
27. Lu, M. and G.R. McDowell, *Discrete element modelling of railway ballast under triaxial conditions.* Geomechanics and Geoengineering: An International Journal, 2008. **3**(4): p. 257-270.
28. Lim, W. and G. McDowell, *Discrete element modelling of railway ballast.* Granular Matter, 2005. **7**(1): p. 19-29.
29. McDowell, G.R., et al., *Laboratory simulation of train loading and tamping on ballast.* Proceedings of the Institution of Civil Engineers - Transport, 2005. **158**(2): p. 89-95.
30. Indraratna, B., P.K. Thakur, and J.S. Vinod, *Experimental and numerical study of railway ballast behavior under cyclic loading.* International Journal of Geomechanics, 2009. **10**(4): p. 136-144.
31. Lobo-Guerrero, S. and L.E. Vallejo, *Discrete element method analysis of railtrack ballast degradation during cyclic loading.* Granular Matter, 2006. **8**(3): p. 195-204.
32. Tutumluer, E., et al. *AREMA gradations affecting ballast performance using discrete element modeling (DEM) approach*. in *Proceedings of the AREMA 2009 Annual Conference, Chicago, Illinois, September*. 2009.
33. Boler, H., Y. Qian, and E. Tutumluer, *Influence of Size and Shape Properties of Railroad Ballast on Aggregate Packing: Statistical Analysis.* Transportation Research Record: Journal of the Transportation Research Board, 2014(2448): p. 94-104.
34. Lu, M. and G. McDowell, *The importance of modelling ballast particle shape in the discrete element method.* Granular matter, 2007. **9**(1-2): p. 69.
35. Zhou, T.Y., et al. *Discrete Element Method Analysis of Mechanical Properties of Railway Ballast during Tamping Process under Different Amplitude*. in *Applied Mechanics and Materials*. 2012. Trans Tech Publ.

36. Taoyong, Z., et al., *Discrete Element Method Analysis of Mechanical Properties of Railway Ballast during Tamping Process under Different Vibration Frequency.* Applied Mechanics and Materials, 2012. **190**: p. 191.
37. Taoyong Zhou, B.H., Junfeng Sun and Bo Yan, *Discrete Element Method Study on the Evolution of Contact Force inside Railway Ballast under Tamping Operation*, in *4th International Conference on Computer, Mechatronics, Control and Electronic Engineering*. 2015.
38. Saussine, G., et al. *Compaction of Railway Ballast During Tamping Process: a Parametric Study*. in *AIP Conference Proceedings*. 2009. AIP.
39. Perales, R., et al. *Numerical investigation of the tamping process*. in *9th World Congress on Railway Research-WCRR*. 2011.
40. Saussine, G., et al. *Numerical modeling of the tamping operation by Discrete Element Approach*. in *World Congress Rail Research*. 2008.
41. Perales, R., G. Saussine, and F. Radjai. *OPTIMIZATION OF THE TAMPING PROCESS TO REDUCE TRACK SETTLEMENT*. in *7th Euromech Solid Mechanics Conference*. 2009.
42. Wang, X., et al., *Study on Discrete Element Modeling Simulation of the Railway Ballast Tamping.* International Journal of Digital Content Technology and its Applications, 2012. **6**(23): p. 660.
43. Thakur, P., J.S. Vinod, and B. Indraratna. *Effect of particle breakage on cyclic densification of ballast: A DEM approach*. in *IOP Conference Series: Materials Science and Engineering*. 2010. IOP Publishing.
44. Huang, H., et al. *Discrete element modeling of aggregate behavior in fouled railroad ballast*. in *Recent Advancement in Soil Behavior, in Situ Test Methods, Pile Foundations, and Tunneling: Selected Papers from the 2009 GeoHunan International Conference*. 2009.
45. Ferellec, J.-F., et al. *Analysis of compaction of railway ballast by different maintenance methods using DEM*. in *EPJ Web of Conferences*. 2017. EDP Sciences.
46. Laryea, S., et al., *Comparison of performance of concrete and steel sleepers using experimental and discrete element methods.* Transportation Geotechnics, 2014. **1**(4): p. 225-240.
47. Pöschel, T. and T. Schwager, *Computational granular dynamics: models and algorithms*. 2005: Springer Science & Business Media.
48. Navarro, H.A. and M.P. de Souza Braun, *Determination of the normal spring stiffness coefficient in the linear spring–dashpot contact model of discrete element method.* Powder technology, 2013. **246**: p. 707-722.
49. Shäfer, J., S. Dippel, and D. Wolf, *Force schemes in simulations of granular materials.* Journal de physique I, 1996. **6**(1): p. 5-20.
50. Stevens, A. and C. Hrenya, *Comparison of soft-sphere models to measurements of collision properties during normal impacts.* Powder Technology, 2005. **154**(2): p. 99-109.
51. Goldsmit, W., *The Theory and Physical Behavior of Colliding Solids.* Arnold, London, 1960.
52. Marsal, R.J., *Mechanical properties of rockfill.* Publication of: Wiley (John) and Sons, Incorporated, 1973.
53. Abbaspour-Fard, M.H., *Discrete element modelling of the dynamic behaviour of non-spherical particulate materials*. 2000, Newcastle University.

54. Azéma, E., F. Radjai, and G. Saussine, *Quasistatic rheology, force transmission and fabric properties of a packing of irregular polyhedral particles.* Mechanics of Materials, 2009. **41**(6): p. 729-741.
55. Matuttis, H.-G. and J. Chen, *Understanding the discrete element method: simulation of non-spherical particles for granular and multi-body systems*. 2014: John Wiley & Sons.
56. Ricci, L., et al., *Dynamic behaviour of ballasted railway tracks: A discrete/continuous approach.* Computers & Structures, 2005. **83**(28): p. 2282-2292.
57. Weaire, D. and T. Aste, *The pursuit of perfect packing*. 2008: CRC Press.
58. Li, S., *Railway sleeper modelling with deterministic and non-deterministic support conditions*. 2012.
59. Remennikov, A.M. and S. Kaewunruen, *A review of loading conditions for railway track structures due to train and track vertical interaction.* Structural control and Health monitoring, 2008. **15**(2): p. 207-234.